THERMOELECTRICITY

QUARTERLY PROGRESS REPORT NO. 3

U. S. NAVY

BUREAU OF SHIPS
WASHINGTON 25, D.C.

OCTOBER, 1962

CONTRACT NObs - 86595
G.O. 81407 - CE

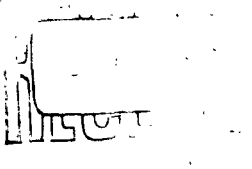

Westinghouse Electric Corporation

CENTRAL RESEARCH LABORATORIES PITTSBURGH 35, PA.

CONTENTS

A. SUMMARY

Work is continuing on the cobalt-antimony system in an effort to develop a matching "p" and "n" material. Thermoelectric property measurements are being extended to higher temperature for the "n" material, and mechanical property measurements are being made. Material having "p" type thermoelectric properties over a broad temperature range has been made, but the properties are not optimum. Most of the contaminents, present as residuals in the raw materials, and those with which the alloy may come into contact during processing, such as O_2 and H_2, have been determined to be "n" type dopes. The "p" doping characteristics of Fe and Sn have been established.

Thermal cycling tests have been run to provide further data on the effects of chemistry and processing on the thermal cracking of GeBiTe. Evaluation was made in terms of change in resistance and microstructure.

Three Reports are appended.

Environmental Suit Generator describes the design, construction, and testing of a thermoelectric heating and ventilating unit developed for the U. S. Army, Contract No. DA-19-129-QM-1981 (OI 6069). It is appended with the permission of Mr. L. A. Spano of the U. S. Army, Natick Laboratories.

Determination of the Figure of Merit of Thermoelectric Materials discusses methods for measuring thermoelectric properties and the errors and accuracies of each.

The Thermal Conductivity of Molten $Cu_2S_{.25}Te_{.7}$ and Molten Cu_2S presents a review

of the method and the results of measurements for these two liquid materials.

B. MATERIAL DEVELOPMENT

Co-Sb Alloy Development

In the program to develop a matching "p" type alloy in the $CoSb_3$ system, a series of alloys have been made in which selected doping elements were added for a portion of the Sb according to the relationship $CoSb_{3-x}M_x$.

The processing method used to make these alloys was to induction melt in a graphite crucible under a protective atmosphere of argon. The molten charge was cast into a water cooled, graphite coated copper mold. Each cast ingot was sealed in an evacuated vycor tube for annealing. Annealing was done at 700°C for times varying from 17 to 65 hours. Raw materials consisted of commercial grade Co briquettes, 99.9% pure (major impurity - 0.24% Ni), and 99.99% pure Sb. Each doping addition was used in its most readily available form. After aging, ingots were crushed to minus 60 mesh powder in a steel mortar and pestle. Pellets were cold pressed at 35 TSI in a carbide lined steel die, then subsequently hot worked at 700°C and 5000 psi in a graphite die under an argon atmosphere.

Room temperature and broad temperature range thermoelectric properties of these alloys are shown in Table 1. Except for magnesium, none of the addition elements resulted in a positive Seebeck under these processing conditions.

The Russian literature* has reported "p" type cobalt antimonide using Fe and Sn doping additions according to the relationship $Co_{1-x}Fe_xSb_3$ and $CoSb_{3-x}Sn_x$. A series of heats were made by the procedure outlined previously in

*Investigation of the Thermoelectric Properties of $CoSb_3$ with Sn, Te, and Ni Impurities, B. N. Zobrina, L. D. Dudkin, A. A. Baikov, Metallurgical Institute, Academy of Sciences, U. S. S. R., Moscow, Dec. 1959.

an attempt to duplicate the results. Also, some combined additions of Sn and Fe were tried. The results, shown in Table 2, verify that Fe and Sn are "p" type dopants. It was also reported by the Russians that Ni is an "n" type dope in these alloys. As was previously stated, the Co used for these experiements contained a major impurity of Ni.

Work at Battelle Memorial Institute has resulted in "p" type $CoSb_3$. The technique was to use spectographic grade Co and to prevent oxygen contamination on the basis that O_2 would be an "n" type dope. To prevent O_2 contamination, the spectographic grade Co powder was outgassed at red heat under a vacuum of 10^{-6} mm Hg. The outgassed cobalt with the Sb was sealed under vacuum in a glass tube for melting. Both cast and hot pressed pellets were evaluated and proved to be strongly "p" type, with Seebeck coefficients of +210 and +195 respectively at room temperature.

In an attempt to deoxidize the cobalt, a heat was made under an hydrogen atmosphere. This heat proved to be very strong "n" type (α = -400μV/°C), indicating possibly that hydrogen is a strong "n" dope.

To avoid the atmosphere problem in the Balzars, all subsequent heats of $CoSb_3$ alloys have been made in evacuated Vycor tubes. For the next series of tube heats, the Co powder was reduced at 1185°C in flowing hydrogen for 3 hours, then outgassed at 1225°C in a 1 x 10^{-6} mm Hg vacuum for 15 minutes. Likewise, the Sb was reduced in static hydrogen at 700°C for 3 hrs. and then outgassed at this temperature for 15 minutes in a 3 x 10^{-4} mm Hg vacuum. Each loaded Vycor tube was evacuated to a 2 x 10^{-5} mm Hg vacuum, and its contents outgassed by heating with a torch before sealing. At 1140°C the charge within the tube was completely molten. After mechanically agitating the tube

to insure homogeneity of the alloy, it was air quenched from this temperature. Compositions investigated and conditions used in this series are listed in Table 3, while results appear in Table 4.

Each variation in the pretreatment of the materials is clearly reflected in the properties of the first three alloys. The changes in the Seebeck coefficient and resistivity are attributed to the presence of oxygen and/or sulfur from the untreated Sb (Alloy 400-2) and of hydrogen from the Co (Alloy 400-3) since it was not outgassed after the reduction. Neither an excess nor a deficiency of one atomic percent Sb (Alloys 400-4 and 400-5 respectively) enhanced the properties of the material. The $CoSb_{2.95}Sn_{.05}$ composition show the effect of Sn doping. In this case the material is probably overdoped. The large dimensional changes during annealing are due to the conversion of the cast structure to the equilibrium structure. A corresponding change occurs in the thermal and electrical properties.

In order to fully evaluate the effects of doping, a series compositions utilizing Sn and Fe as dopants are currently being prepared in Vycor tubing. Other types of doping will also be employed with special emphasis upon lowering the rather high thermal conductivity.

Seebeck and resistivity versus temperature measurements have been made for a series of "n" type Co-Sb-Te-Se alloys. Results are plotted in Figure 1. Room temperature thermal conductivities of the alloys were measured and are as follows:

Alloy	K, W/cm-°C Room Temp.
$CoSb_{2.85}Te_{.03}Se_{.1}$	0.037
$CoSb_{2.8}Te_{.1}Se_{.1}$	0.027
$CoSb_{2.7}Te_{.03}Se_{.27}$	0.035

$CoSb_{2.67}Te_{.03}Se_{.3}$	.034
$CoSb_{2.6}Te_{.1}Se_{.3}$	0.027

Thermal expansion has also been measured and is 10×10^{-6} in/in-°C for the $CoSb_{2.6}Te_{.1}Se_{.3}$ alloy from room temperature to 600°C. In this temperature range, thermal expansion is a straight line function, and a very low heating-cooling hysteresis indicates that the alloy is stable.

TABLE 1

$CoSb_{3-x}M_x$ Alloys

		ROOM TEMPERATURE			ΔT: 450-150°C		
M	x	α (μV/°C)	ρ x 10^3 (Ω-cm)	K (watts)/(cm°C)	$\mathcal{L}$ (μV/°C)	$\bar{\rho}$ x 10^3 (Ω-cm)	Casting Temp. (°C)
-	0.00	-271	15.2	0.0793	-212	10.4	1100
K	0.05	-205	4.08	0.0750	-255	4.77	1170
K	0.15	INGOT DESTROYED DURING AGEING					1160
Ca	0.05	-102	2.12	0.0645	-185	1.72	1110
Ca	0.15	-117	1.95	0.0616	-166	1.54	1174
Ba	0.05	-115	1.52	0.0595	-157	1.26	1152
Ba	0.15	-61	0.39	0.0624	-93	0.36	1130
Ti	0.05	-177	4.71	0.0684	-268	4.43	1232
Ti	0.15	-104	37.0	0.0867	-3	10.7	1242
Mg	0.05	-164	95.0	0.0841	+32	19.6	1124
Mg	0.15	-123	25.0	0.0859	-64	11.3	1144

TABLE 2

$Co_{1-x}Fe_xSb_3$ $CoSb_{3-x}Sn_x$ $Co_{1-x}Fe_xSb_{3-x}Sn_x$ Alloys

		ROOM TEMPERATURE			ΔT: 450-150°C	
Dopant	x	α (μV/°C)	$\rho \times 10^3$ (Ω-cm)	K (watts/cm-°C)	$\bar{\alpha}$ (μV/°C)	$\bar{\rho} \times 10^3$ (Ω-cm)
Fe	0.01	+67	3.59	0.0959	+142	3.84
Fe	0.05	+25	0.87	0.058	+84	1.42
Sn	0.0015	-232	14.9	0.0833		
Sn	0.003	-180	140.0	0.0883		
Sn	0.005	-268	85.0	0.086		
Sn	0.007	+43	0.88	0.0952	+101	1.87
Sn	0.01	+26	0.60	0.0918	+89	1.39
Sn	0.02	+12	0.49	0.0692		
Sn	0.03	+8	0.56	0.0635		
Sn	0.04	+5	0.57	0.0523		
Sn	0.05	+24	0.60	0.0469	+66	1.25
Sn	0.06	+5	0.64	0.0414		
Sn	0.07	+5	0.65	0.0383		
Sn	0.10	+3	0.71	0.0320		
Fe/Sn	0.01/0.005	+41	0.93	0.087	+107	1.89
Fe/Sn	0.01/0.03	+12	0.64	0.0502	+70	1.31
Fe/Sn	0.02/0.005	+25	0.70	0.071	+79	1.45

TABLE 3

Alloy No.	Formula	Conditions
400-1	$CoSb_3$	H_2 reduced, vacuum outgassed Co and Sb.
400-2	$CoSb_3$	H_2 reduced, vacuum outgassed Co and untreated Sb.
400-3	$CoSb_3$	H_2 reduced Co and H_2 reduced, vacuum outgassed Sb.
400-4	$CoSb_{3.04}$	H_2 reduced, vacuum outgassed Co and Sb.
400-5	$CoSb_{2.96}$	H_2 reduced, vacuum outgassed Co and Sb.
400-6	$CoSb_{2.95}Sn_{.05}$	H_2 reduced, vacuum outgassed Co and Sb. H_2 reduced Sn.

TABLE 4

Alloy No.	AS CAST: Room Temperature α μV/°C	AS CAST: Room Temperature ρ Ω-cmx10^{-3}	AS CAST: Room Temperature K W/cm-°C	AS CAST: ΔT: 550-150°C $\tilde{\alpha}$ μV/°C	AS CAST: ΔT: 550-150°C ρ Ω-cmx10^{-3}	ANNEALED AT 700°C FOR 22 HOURS: Room Temperature $\tilde{\alpha}$ μV/°C	ANNEALED AT 700°C FOR 22 HOURS: Room Temperature ρ Ω-cmx10^{-3}	ANNEALED AT 700°C FOR 22 HOURS: Room Temperature K W/cm-°C	ANNEALED AT 700°C FOR 22 HOURS: ΔT: 550-150°C $\tilde{\alpha}$ μV/°C	ANNEALED AT 700°C FOR 22 HOURS: ΔT: 550-150°C ρ Ω-cmx10^{-3}	% Increase in Dia.
400-1	+23	0.14	0.153	+9	0.18	+98	4.65	0.0436	+143	7.69	12.0
400-2	+23	0.18	0.146			+61	1.86	0.0695	+116	3.01	3.9
400-3	+23	0.16				+127	28.7	0.0471	+100	7.23	7.6
400-4	+23	0.14				+79	8.11	0.0306	+133	10.5	15.9
400-5	+22	0.12				+35	1.50	0.0453	+96	3.96	17.3
400-6	+6	0.18		+5	0.62	+24	0.54	0.0680	+76	1.63	3.6

All units are same as in Table 1 and 2.

CURVE 565326

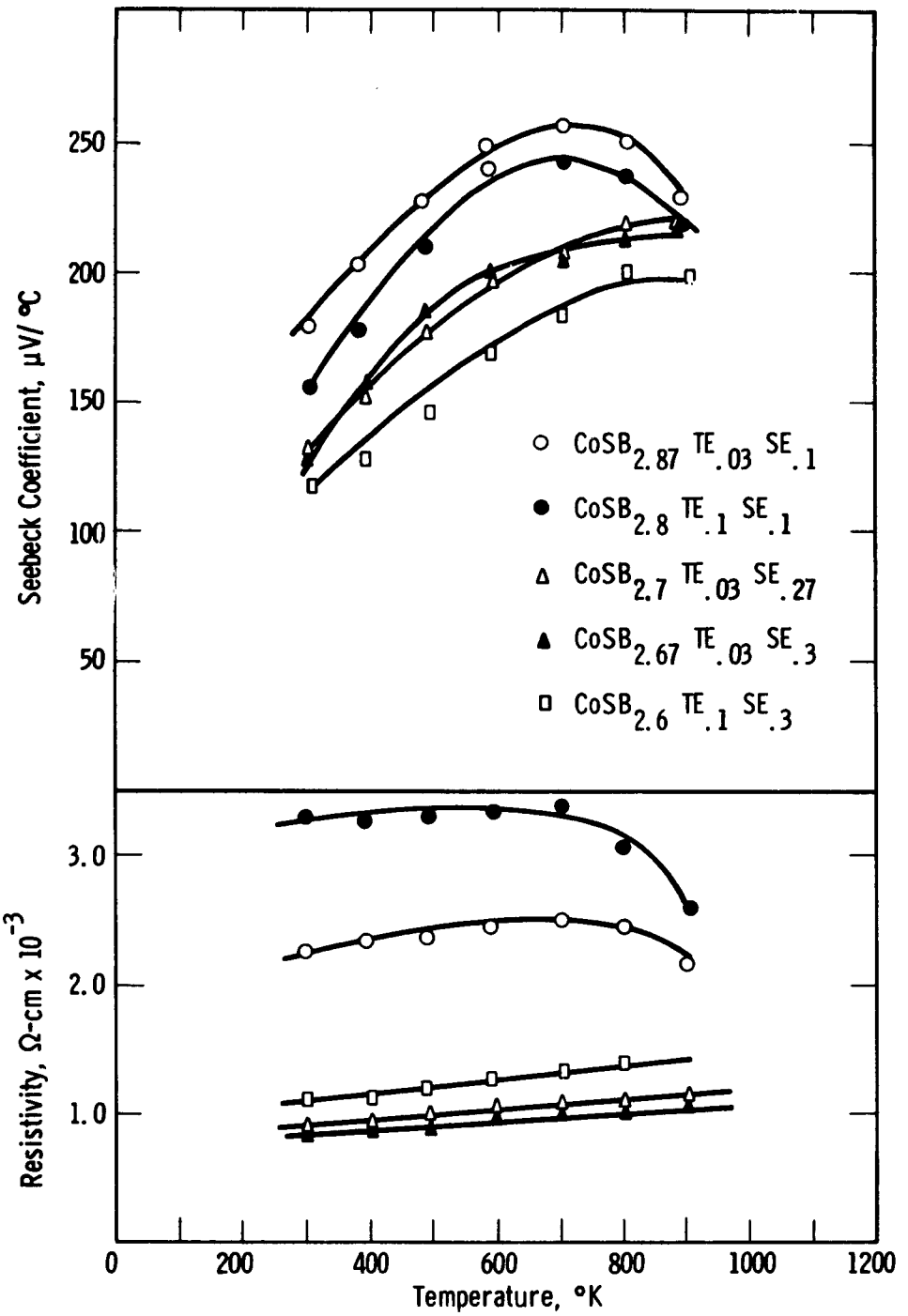

Fig. 1—Seebeck and resistivity of cobalt antimony tellurium selenium alloys

Ge-Bi-Te Evaluation

As a part of the program to improve the life-performance properties of materials, thermal cycling tests are being run on GeBiTe with variations in chemistry and processing. In the following section, results for two compositions, $Ge_{.93}Bi_{.07}Te$ and $Ge_{.95}Bi_{.05}Te$, for which the time and temperature of sintering were varied, are presented.

Cyclic testing consisted of heating one end of a 1/2 inch diameter x 1/2 inch long pellet to establish a 450°C-100°C temperature gradient along the pellet, and then cooling to a "no gradient" condition. Heating and cooling rates were such as to provide one cycle per hour including 15 minutes at temperature. Testing was done in an argon atmosphere.

Performance in cycling was evaluated by measuring both room temperature and broad temperature range Seebeck and resistivity, and by micro examination. Because of the possibility of reaction from the liquid contacting alloy used for α and ρ measurements, control pellets were used for the "before" measurements. Between-pellet property variations for the same heat processed in the same manner are normally of the order of 5 percent. Compositions, heat numbers, and sintering treatments for this test run are given in Table 1.

Table 2 gives the broad temperature range property results for the cycling tests. The table has been arranged in order of increasing sintering temperature. Perhaps the most significant indication is that essentially all of the samples showed an increase in resistance. The percent change shown in Table 2 may be more or less by an amount equivalent to the between-pellet variation of the control and test sample. There does not appear to

be any trend of increased cycle resistance with increasing sintering temperature in the resistance measurements. There is considerable between-heat variation. Heat 3365 has an average percent change four times greater than the other three heats. There is a clear indication that raising the final sintering temperature lowers the Seebeck and the resistivity within a heat. Other work* has shown that raising the sintering temperature raises the strength and modulus.

Microstructure examinations showed that thermal cycling caused cracks to form in all of these samples. Figures 1 and 2 show the before and after microstructure of Heat 3365 ($Ge_{.93}Bi_{.07}Te$) and Heat 3418 ($Ge_{.95}Bi_{.05}Te$). Both samples are the 685°C sinter condition. There was a tendency for the samples with higher sintering temperatures to be less severely cracked, indicating a possible improvement of thermal cycling resistance by additional modification of processing treatments.

The phase change in GeBiTe complicates any evaluation of resistance change with time. Each phase has a different resistance, and the resistance of a pellet will be dependent on the proportions of the phases present. The proportions of the phases are in turn dependent on the recent time-temperature conditions to which the pellets has been subjected. To lessen this effect for these tests, the cycled samples were annealed at 350°C (above the phase change) and fast cooled after the thermal cycle tests. This condition corresponds to the "as processed" condition.

Work towards improving the thermal cycle resistance of GeBiTe, is continuing. Preliminary results indicate improvement from higher temperature sintering and change in particle size.

---

*Module Improvement Program, Final Report, October 1962
NObs 84329

TABLE 1

SUMMARY OF CYCLING TESTS ON GeBiTe

Composition	Heat No.	Sample No.	Sintering Treatment
$Ge_{.93}Bi_{.07}Te$	3365	1 & 2	1-1/2 hr. at 600°C, H_2 + 1/2 hr. at 665°C, H_2
"	"	3 & 4	1-1/2 hr. at 600°C, H_2 + 1/2 hr. at 680°C, H_2
"	"	5 & 6	1-1/2 hr. at 600°C, H_2 + 1/2 hr. at 685°C, H_2
"	3417	12, 13	1-1/2 hr. at 600°C, H_2 + 1/2 hr. at 665°C, H_2
"	"	7	1-1/2 hr. at 600°C, H_2 + 1/2 hr. at 675°C, H_2
"	"	8	1-1/2 hr. at 600°C, H_2 + 1/2 hr. at 680°C, H_2
"	"	9, 14, 15	1-1/2 hr. at 600°C, H_2 + 1/2 hr. at 685°C, H_2
"	3366	10	1-1/2 hr. at 600°C, H_2 + 1/2 hr. at 675°C, H_2
"	"	11	1-1/2 hr. at 600°C, H_2 + 1/2 hr. at 685°C, H_2
$Ge_{.95}Bi_{.05}Te$	3418	16, 17	3 hrs. at 600°C, H_2
"	"	18, 19, 20	1-1/2 hr. at 600°C, H_2 + 1/2 hr. at 685°C, H_2

TABLE 2

BROAD TEMPERATURE RANGE PROPERTIES OF 450°C-100°C THERMAL CYCLED GeBiTe

Sample No.	Heat No.	CONTROLS (NO CYCLES) $\bar{\alpha}$, μV/°C 450°C-100°C	CONTROLS (NO CYCLES) $\bar{\rho}$, Ω-cm x 10^3 450°C-100°C	AFTER 100 CYCLES & ANNEALING $\bar{\alpha}$, μV/°C 450°C-100°C	AFTER 100 CYCLES & ANNEALING $\bar{\rho}$, Ω-cm x 10^3 450°C-100°C	Percent Change $\bar{\alpha}$	Percent Change $\bar{\rho}$	Maximum Sintering Temperature °C
16	3418	+158	2.00	+147	1.88	-7	-6	600
17	3418	+158	2.00	+152	2.24	-4	+12	"
1	3365	+186	2.69	+171	2.86	-8	+6	665
2	3365	+186	2.69	+177	3.12	-5	+20	"
12	3417	+195	2.17	+177	2.35	-9	+8	"
13	3417	+195	2.17	+177	2.40	-9	+11	"
7	3417	+191	2.13	+184	2.44	-4	+13	675
10	3366	+185	2.24	+181	2.64	-2	+18	"
3	3365	+181	1.55	+184	2.93	+2	+90	680
4	3365	+181	1.55	+188	2.19	+4	+41	"
8	3417	+186	1.52	+192	1.81	+3	+19	"
5	3365	+182	1.37	+190	2.05	+4	+49	685
6	3365	+182	1.37	+188	1.68	+3	+23	"
9	3417	+180	1.49	+192	1.66	+7	+11	"
14	3417	+180	1.62	+175	1.61	-3	0	"
15	3417	+180	1.62	+178	1.52	-1	-6	"
11	3366	+185	1.51	+194	1.71	+5	+13	"
18	3418	+157	1.21	+156	1.48	0	+22	"
19	3418	+157	1.21	+159	1.40	+1	+16	"
20	3418	+157	1.21	+167	1.37	+6	+13	"

Neg. No. 41552 Mag. 100 X

Heat 3365, $Ge_{.97}$ $Bi_{.03}$ Te Sintered at 685°C

Control sample

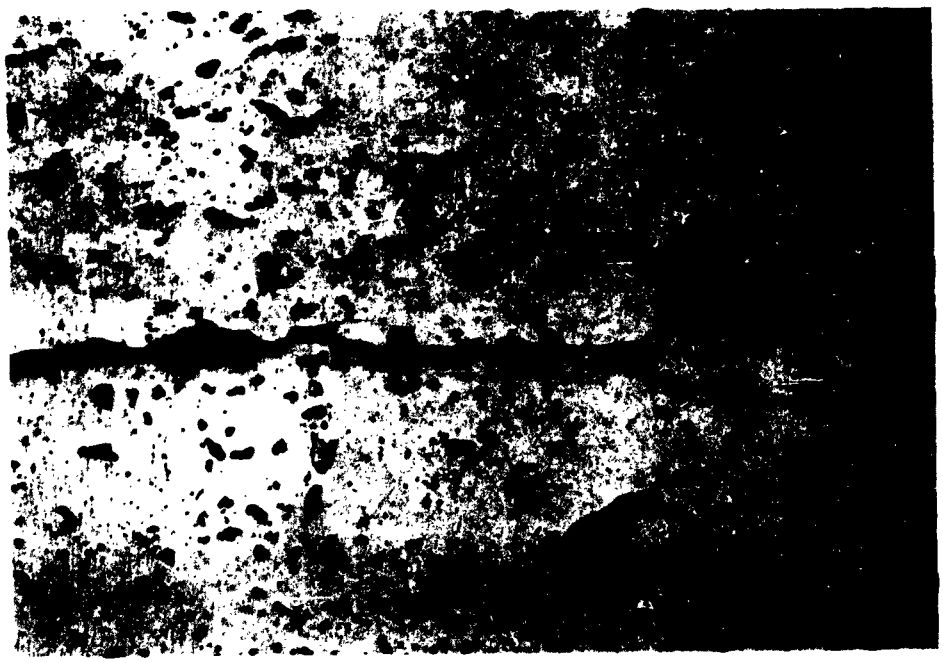

Neg. 41553 Mag. 100 X

Heat 3365, $Ge_{.97}$ $Bi_{.03}$ Te Sintered at 685°C

After 100 thermal cycles, 450°C-100°C

Figure 1

Neg. No. 41561 100 X
Heat 3418, $Ge_{.95}$ $Bi_{.05}$ Te, Sintered at 685°C

Neg. No. 41559 100 X
Heat 3418, $Ge_{.95}$ $Bi_{.05}$ Te, Sintered 685°C
After 100 Thermal cycle 450-100°C

Figure 2

The following section describes the design, construction, and preliminary testing of a thermoelectric heating and ventilating unit built in partial fulfillment of Contract DA 19-129-QM-1981 (OI 6069) for the United States Army. Acknowledgement for permission to append this report is due Mr. L. A. Spano, Head, Advanced Projects, Clothing and Organic Materials Division, U. S. Army, Natick Laboratories, and Mr. W. D. Pouchot, Advisory Engineer responsible for the project at Westinghouse Central Laboratories.

The purpose for appending this report is twofold: the thermoelectric material and couple technology that made design and construction of this unit possible is a result of the program jointly sponored by the United States Navy, Bureau of Ships, and Westinghouse Electric Corporation, and the development of this unit proves another practical application for thermoelectricity.

Introduction

An engineering model of a thermoelectric heating and ventilating unit has been fabricated, subjected to limited performance tests, and delivered to the U. S. Army, Natick Laboratories under Phase I of Contract DA 19-129-QM-1981 (OI 6069). The prime purpose of such a unit is to provide a flow of air to be used in heating or ventilating a combat clothing ensemble to keep troops in thermal balance when operating in extreme environments, and when exposed to enemy imposed hazards.

In the recently delivered unit this flow of air is provided by a centrifugal blower driven by a d.c. motor. The electric power for the motor is obtained from a thermoelectric generator operated on propane fuel. Heating of the flow of air for the suit, when desired, is obtained by utilizing the waste heat from the generator.

The engineering objectives for this Phase I model were to be within 20% of the following levels of performance:

(1) Continuous operation at maximum output without refueling - not less than eight (8) hours.

(2) Weight limitation for complete unit, fully fueled - not more than thirteen (13) pounds.

(3) Usable output to the combat clothing is to be no less than 12 CFM of air at STP and at 4" H_2O positive static pressure.

In addition to fulfilling its prime function of an air supply, the unit may be used as an independent source of energy for equipment using a modest amount of electrical power (20 watts) by switching off the suit blower motor and attaching auxiliary power leads to terminals provided. Direct

connection to the generator gives 10 volt d.c. 110 volt a.c. may be obtained by using an inverter. A 15 watt inverter was supplied with the unit.

The unit might also be used as a single burner 'cook' stove with a slight modification.

Description of Unit

A plan view layout of the unit is shown in Figure I. Looking at this view, combustion air and cooling air for the generator enters the generator blower. From this blower the air flows into a plenum at the left hand end of the generator. All but 1 CFM of this air flows through the heat exchanger on the cold side of the thermocouples to the right hand side of the generator where it either is exhausted to ambient or is partially deflected by a grid valve into a duct leading to the filter case and thence into the inlet of the suit blower. Under normal operating conditions this air leaving the generator is about 100°C, (212°F) so that even when heating is desired, ambient air must be mixed with it to bring it to a temperature suitable for humans. The mix of heated and ambient air is controlled by a flipper valve shown at the lower right of the plan view acting in unison with the grid valve. These two valves are turned by means of the control knob adjacent to the flipper valve. In this figure ambient air is called ventilating air. The heated and ambient air mix in the filter case and are drawn into and through the suit blower conditioned for entrance into a suit.

One CFM of generator air is used as combustion air. This air is directed around the unit from left to right and enters a hollow bullet mounted on the center line of the unit. The fuel also enters at this location. The fuel and combustion air flow to the left hand end of the unit where they mix in a bunsen type aspirator. The mixture then exhausts into the annular space between the

central bullet and core through a screen which acts as a flameholder. The combustion products flow back through the annular space and are exhausted to atmosphere on the right hand end of the generator. The amount of combustion air is controlled by orifices at the inlet of the combustion air by-pass tube. The fuel flow is controlled by the fuel pressure regulator at the lower right hand side of the unit.

The actual physical appearance of the unit is shown in the photographs of Figures 2, 3, 4, and 5. Figure 2 is a back view of the unit and corresponds to the plan view of Figure 1. The cover of the filter box has been removed to show the suit blower motor and underneath it, the inlet to the blower. The blower itself is not visible as it lies back of the filter case. Also visible in the filter case are two switches controlling the generator and blower motor electrical circuitry.

Figure 3 corresponds to the right elevation view of Figure 1. Prominantly displayed in this view are the grid valve, the air adjustment knob and linkage between the two. Also visible is the combustion air tube, fuel tube and the combustion products exhaust. The adjustment lug on the fuel pressure regulator and electrical leads from the generator can also be seen. The sleeve with knob over the combustion air tube covers a slot which is open during starting of the unit.

Figure 4 corresponds to the left elevation view of Figure 1. A part of the scroll of the suit blower can be seen under the black casing of the generator blower. The wires coming from the generator are for temperature measurement of the hot side core.

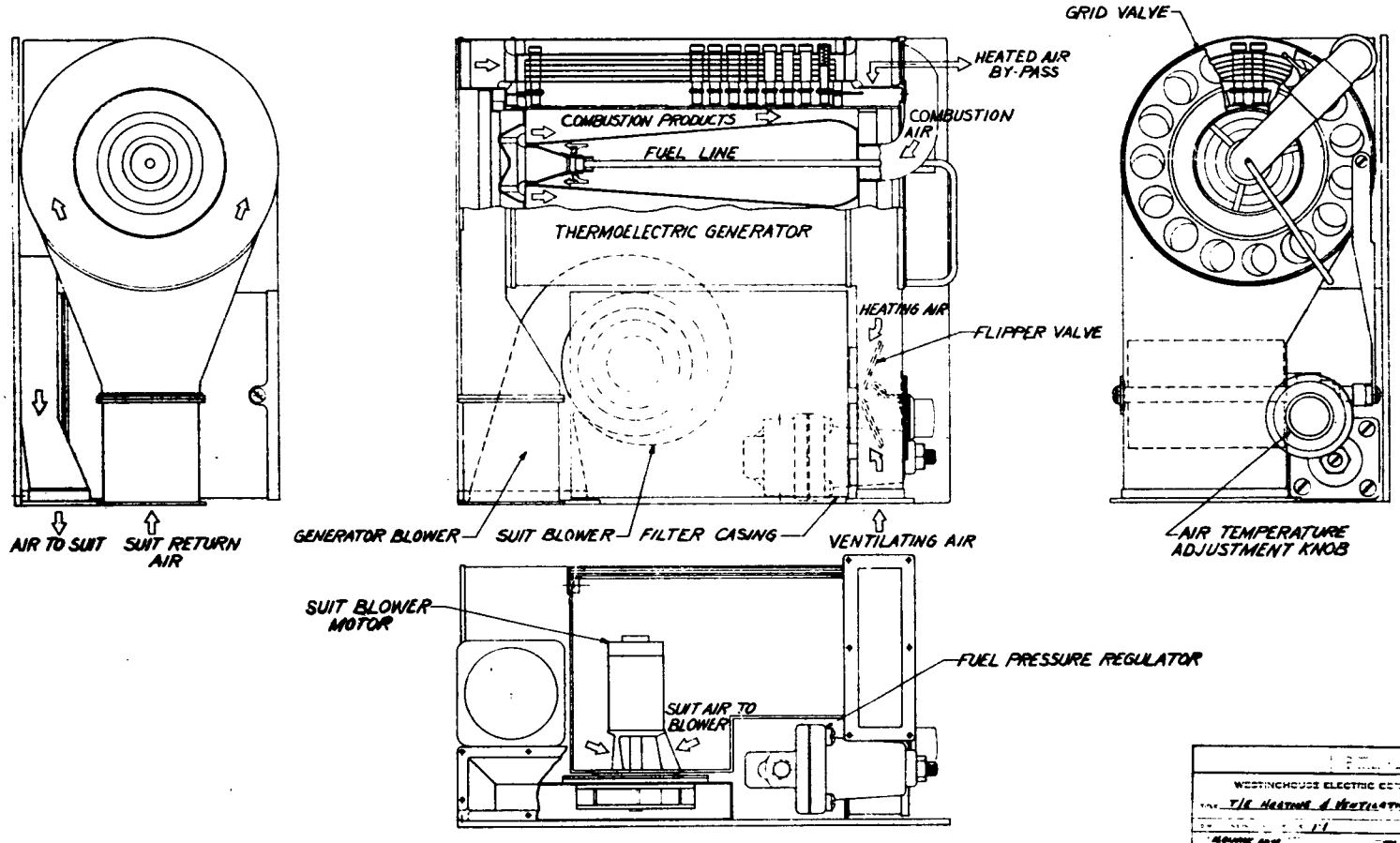

FIG. 1 - THERMOELECTRIC HEATING AND VENTILATING UNIT

WESTINGHOUSE ELECTRIC CORPORATION
T/E Heating & Ventilating Unit
7530809

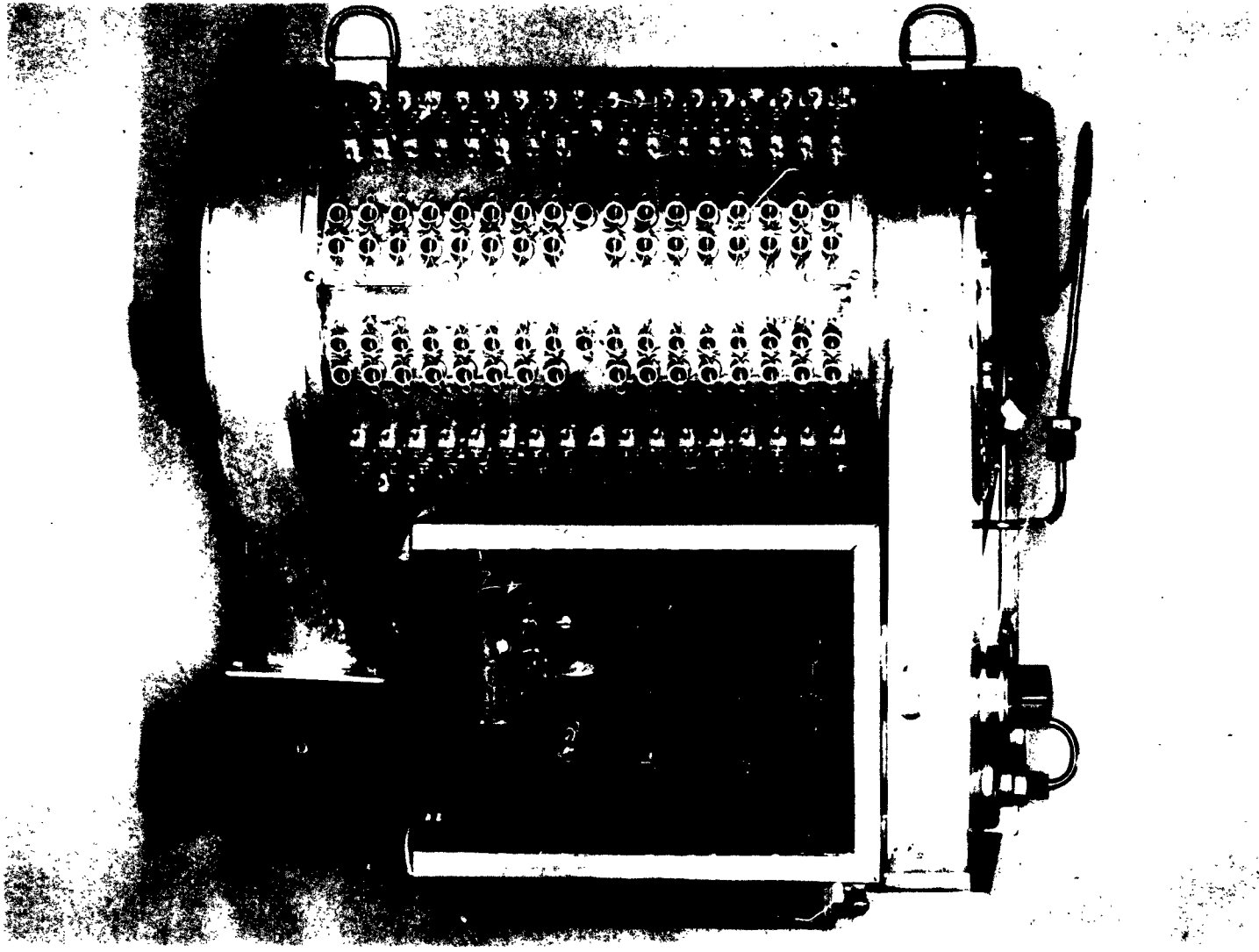

FIGURE 2. Backview, Heating, and Ventilating Unit

CLM 25344

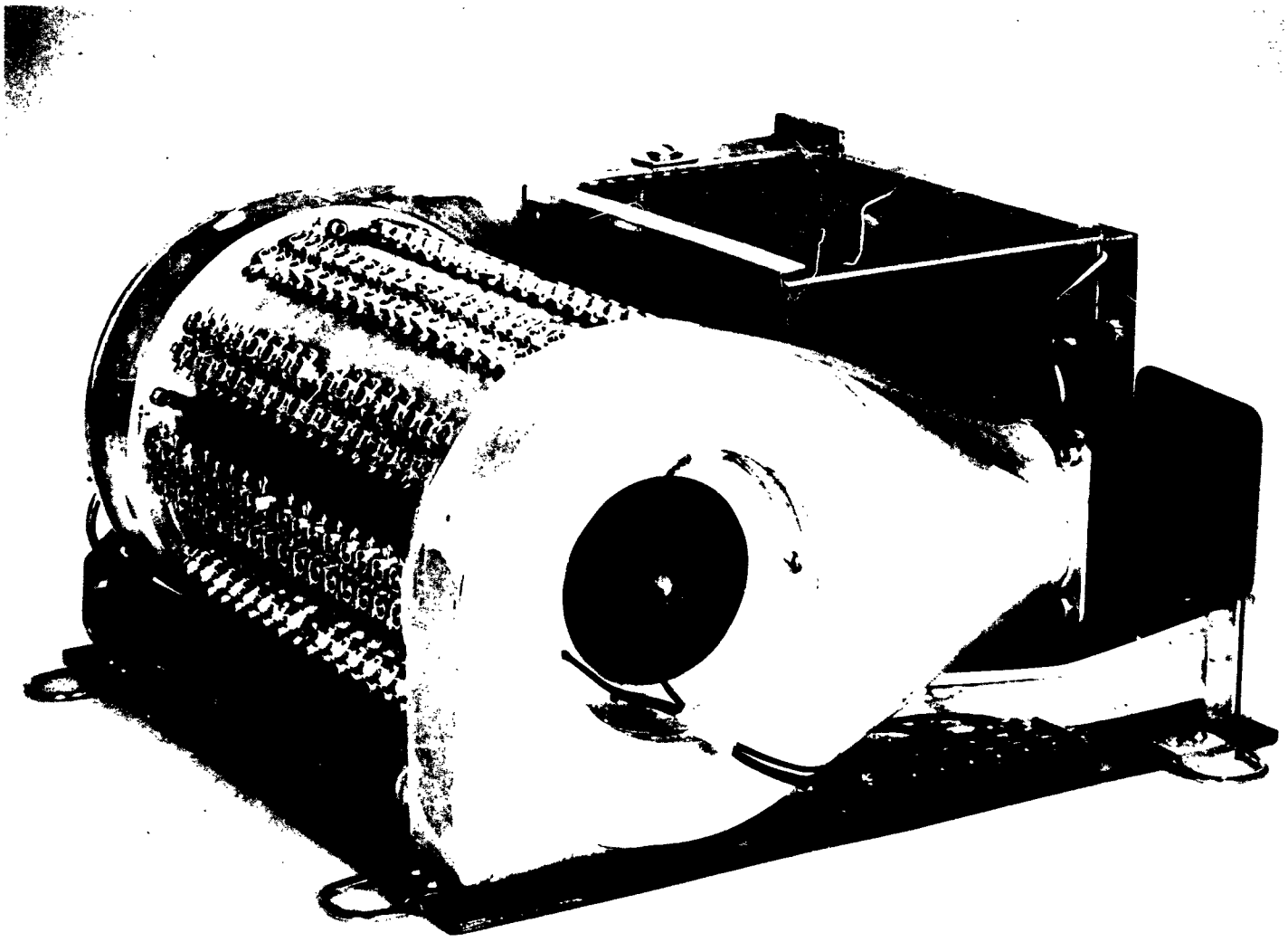

FIGURE 3. Right Side View, Heating and Ventilating Unit

CLM 25343

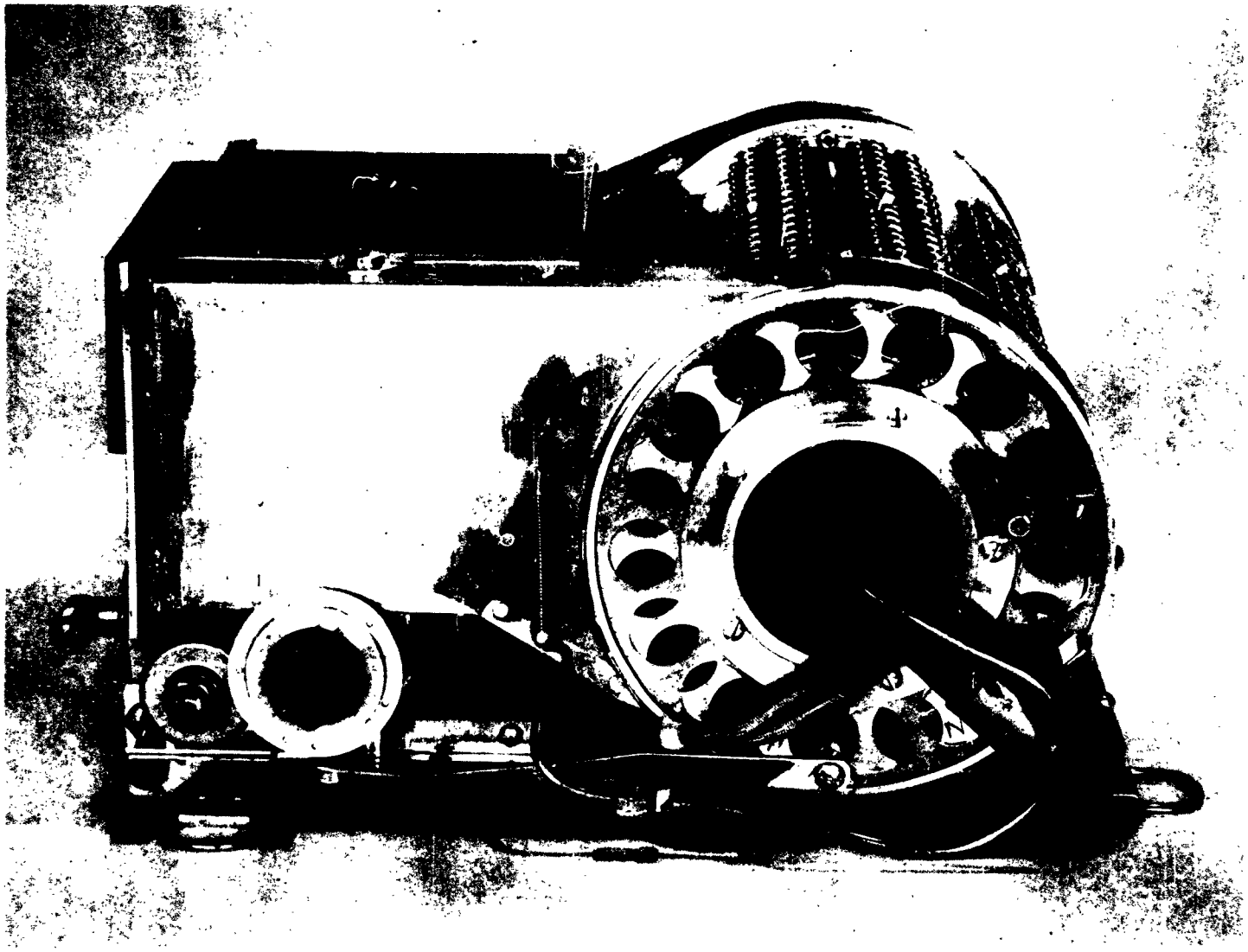

FIGURE 4. Left Side View, Heating and Ventilating Unit

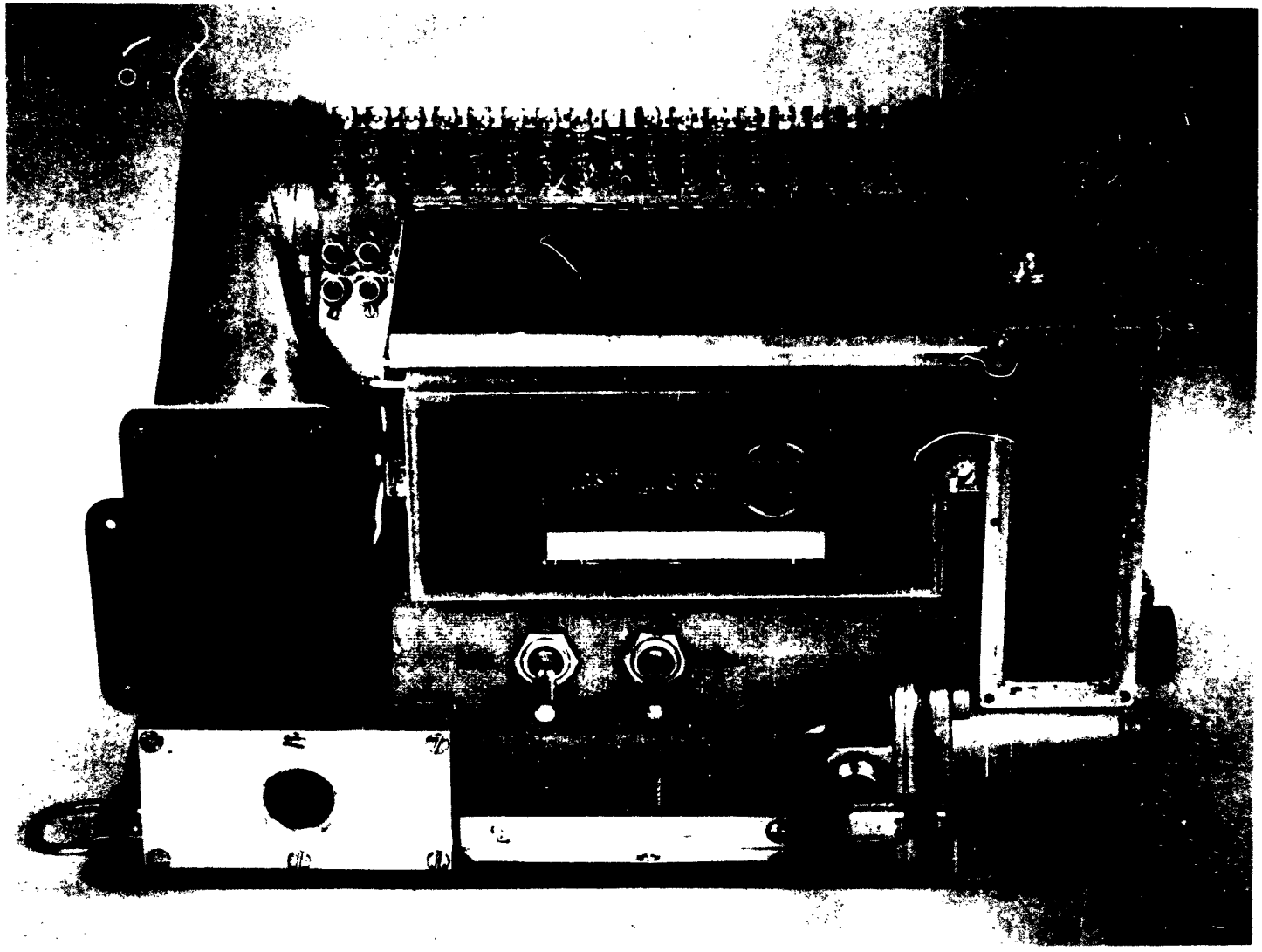

FIGURE 5. Bottom View, Heating and Ventilating Unit

CLM 25341

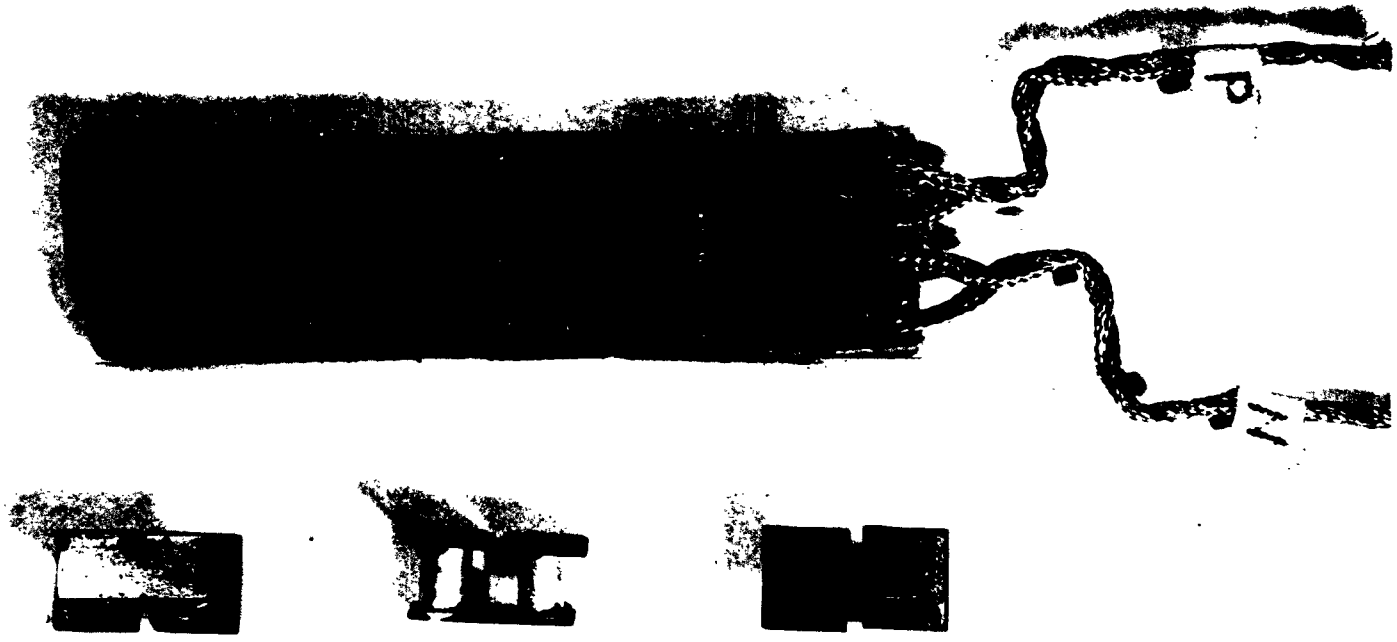

FIGURE 6. Typical Thermoelectric Module and Couples

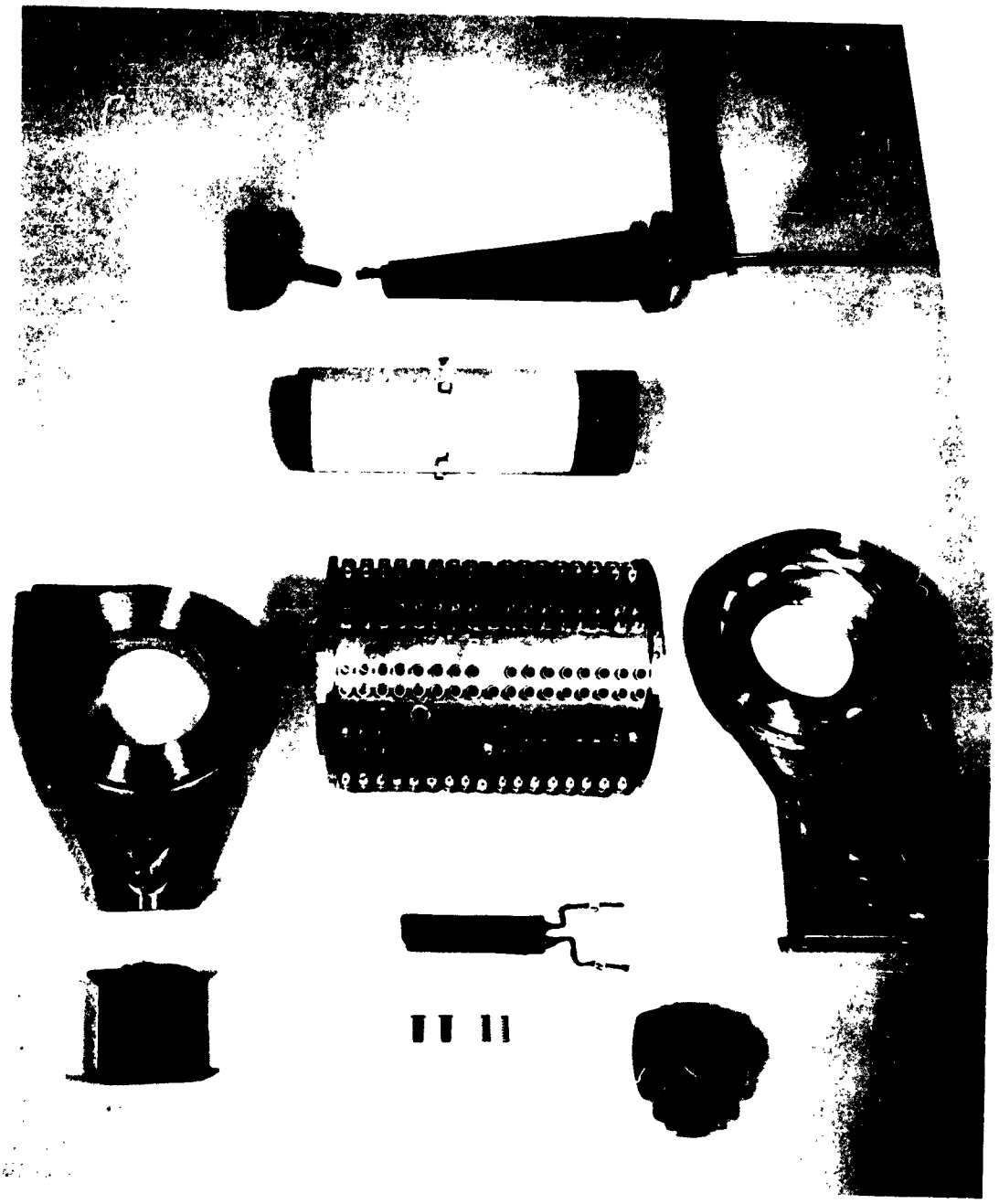

FIGURE 7. Pre-assembly View of Generator Parts

Figure 5 corresponds to the bottom elevation view of Figure 1 and is the bottom of the unit as mounted on a man's back. Visible on the right hand side is the fuel pressure regulator and the inlet for the ventilating air. The fuel line from the fuel tanks is attached at the elbow visible in front of the pressure regulator. Moving to the left the switches which turn the generator power (Gen) and suit blower (Fan) off and on are visible. Just above these switches is a terminal board covered by a small housing. Two auxiliary power takeoffs are available in this terminal box with the cover removed. At the far left is the exit of the suit blower and the entrance to the generator blower. The suit blower exit is covered with an orifice plate which would be removed for actual operation with a suit.

The dimensions of the unit, exclusive of the rings for mounting to the suit harness but including protruding knobs and fuel tube, are 10-1/2" x 10-1/2" x 5". The weight of the unit without fuel supply is 10.35 pounds. The weight of the system including two propane torch bottles with approximately 7-1/2 hour fuel supply, flex hose, and valves for belt mounting of the fuel bottles is 15.21 pounds.

Operating the Unit

a. Startup

This unit has been supplied with a flexible fuel line with two propane torch bottle valves attached. After making sure that the valves are closed and that the flex line connection to the unit is tight, screw a propane torch bottle into each valve. Then

(1) Open the grid valve (Fig. 3) by turning the hot air control knob (Fig. 3) as far as it will go in a clockwise direction

with moderate hand pressure.

(2) Turn generator switch (Gen., Fig. 5) to 'on' and turn fan switch (Fan, Fig. 5) and converter switch, if supplied, to 'off'.

(3) Uncover slot in combustion air tube by sliding the sleeve over this tube upwards (Fig. 3).

(4) Open fuel valves, completely. Insert lighted match in front of burner exhaust (Fig. 3). A weak flame will flash back into the burner.

(5) When the generator blower (Fig. 5) starts to turn over (approximately 1 minute) close the air slot in the combustion air tube by sliding the sleeve downwards until the slot is covered.

(6) Wait 5 minutes more by the clock. Turn fan switch (Fan, Fig. 5) to 'on' if suit air is desired or alternately turn on converter switch if auxiliary power (15 watts) is desired.

(7) Suit air may be heated by rotating the hot air control knob in a counterclockwise direction. An adjustment of the temperature of the air coming from the unit's suit fan should be made before attaching to the suit otherwise an unpleasantly hot or cold 'shower' may result.

NOTE: The thermal response of this unit to changes in control know position will be slow. Several minutes should be allowed after a change in position to make sure the unit has come to a new equilibrium temperature.

b. Shutdown

(1) Disconnect the unit from the suit leaving the suit fan running.

(2) Turn off the fuel valves completely.

(3) Wait 1 minute. Turn suit fan switch (Fan, Fig. 5) to 'off'.

(4) When generator fan has come to a stop (about 5 minutes more), the unit may be stored in a clean dry location.

Component Discriptions

a. Generator Details

The basic component of the generator is, of course, the thermocouple. Figure 6 shows several individual couples and a module of 8. The generator contains 20 of these 8 couple modules or a total of 160 couples. The entire 160 couples are connected in series.

Looking at the individual couples, the left hand couple gives a view from the hot side of the generator. The center couple is a side view and the right hand couple shows a view from the cold side of the generator. The hot strap and the two cold side caps are of 1/32" thick Armco Iron. The dimensions of the hot side strap are 1/4" x 5/8". The dimensions of the cold caps are 5/16" x 3/8". The thermoelectric legs are 3/16" dia. x 1/4" long. The 'P' leg is a 95% GeTe - 5% Bi_2Te pressed and sintered material. The 'N' leg is a Bi doped PbTe pressed and sintered material. These legs are positioned on the hot strap on 3/8" centers. The 'P' leg is joined to the strap and its cap by a furnace braze at 680°C in hydrogen, nitrogen, and argon using Nicrobraze as the joining alloy. The 'N' leg is joined to the strap and its cap by a furnace braze in nitrogen at 725°C using a gold-zinc alloy. Graphite fixtures are used to hold the pieces during brazing. The legs of the couples are coat-

ed with Sicon Aluminum paint to increase resistance to atmospheric attack.

As stated previously a module consists of 8 couples. The couples are connected electrically by soldering braided wire on the under side of the cold side caps. These wires are visible in the breaks between couples in Fig. 6. Insulation around and between the couples is provided by Johns-Mansville Cerafelt. For external handling of the module during assembly, the Cerafelt was basted with cotton thread.

The modules are mounted on the flats of the central core shown in Fig. 7. This is a picture of some of the various component parts of the generator. The central core is the ten-sided object with a white plasma sprayed aluminum oxide coating. Just below this core is the burner assembly. Above the core is the cold side heat exchanger and to the right and left of the heat exchanger are the inlet and exit plenums respectively. Above the thermoelectric module are two typical cold side thermocouple followers and springs and to the right of these is the generator blower-motor assembly. To the left is a fuel pressure regulator.

A better idea of the actual assembly arrangement can be obtained by referring back to Fig. 1. As can be seen the burner is mounted inside the central core and the thermocouples are pressed against this core by individual followers protruding into the hollow pins of the cold side heat exchanger. These followers are under spring compression. This compression is actually provided by cotter-keys as shown in Fig. 2 rather than caps as drawn in Fig. 1.

The heat flow path is from the burner to the core to the thermocouple strap through the legs and followers to the cold side heat exchanger

pins and cylindrical fins and then to the generator cooling air. The heat exchanger is positioned relative to the core by means of 5 radial pins inserted through 5 of the hollow pins, located in the center of the generator lengthwise, into the legs visible on the core in Fig. 7. Electrical insulation along this path is provided on the hot side of the thermocouples by the aluminum oxide layer on the core plus a 2 mil mica layer between this layer and the thermocouple hot strap. On the cold side of the thermocouple, electrical insulation is provided by a 'hard coat' on the aluminum followers plus silicone grease over the followers. The grease also reduces the sliding friction on the followers.

The main effort in this design is to provide minimum restraint between the couples and related parts during relative thermal expansion of these pieces under transient operation with isolation of the thermocouples from external loads and shocks. This is mandatory because the tensile strength of the 'P' thermoelectric material is less than 400 psi at 450°C and its resistance to mechanical shock is low.

The burner bullet and head were made from .018" Inconel sheet. The burner screen is 24 mesh, .011" dia. wire of 25-20 stainless. The fuel tube is 18-8 stainless. The core was machined from a bar of Alcoa M-470 aluminum compact material and 'hardcoated'. The 'hardcoat' was very porous. Because of this porosity the 'hardcoat' was sand blasted off and sprayed aluminum oxide layer substituted.

The thermocouple followers were machined from 24T6 aluminum and hardcoated.

The springs were made from bronze wire and exert a pressure of approximately 15 psi on each thermocouple.

The cold side heat exchanger parts were joined together by aluminum dip brazing. Prior to dip brazing the pins were held in place by mechanically expanding them into the cylindrical fins. The cylindrical fins and flanges were held in place by rivets. The pins were of #24T6 aluminum tube initially solution heat treated to 'TO' for ease of expanding into the cylinders and age-hardened back to T6 after dip brazing prior to final machining. The cylindrical fins were from .015" tk #22 aluminum brazing sheet and the outer casing from .031" tk #21 aluminum brazing sheet. The flanges were of #24T6 aluminum.

The inlet and exit plenums to the generator were made from aluminum of unknown composition and riveted and soldered together.

b. Other Components

The generator blower is a Dean and Benson Vaneaxial Model HF3-1. This blower delivers approximately 27 CFM of 0.25" H_2O static pressure when operated at 9000 rpm.

The suit blower is a backwardly curved centrifugal developed under U. S. Army Contract DA 19-129-QM-1572 and designated as Westinghouse New Products Lab Model MFMP III. This blower delivers approximately 12 CFM at 4" H_2O static pressure when operated at 13,000 rpm.

Both d.c. motors are of the permanent magnet type and manufactured by Globe Industries Inc. The suit blower motor is their Model LL9 and the generator blower motor is their Model MM9. Model LL9 was specified to provide 11,300 $\pm$ 500 rpm at 9 volts and 0.0125 shaft HP output. Model MM9 was

specified to provide 9000 ± 500 rpm at 9 volts and 0.0031 shaft HP output. Because of the way the total system matches, they operate at 10^{+}v and 13,000 rpm and 9,000 rpm, respectively. As the generator performance deteriorates with operating time the voltage will more nearly approach the motors nominal of 9 volts.

The fuel pressure regulator is made by Goss Gas and has Underwriter's Labs approval. It is nominally set for 19 psi gage fuel pressure.

The filter case is constructed of 1/16" thick glass reinforced epoxy plastic. The packboard is of 1/8" thick glass reinforced epoxy plastic.

c. Component Weights

Fuel System			5.74 lb.
	Fuel	1.8 lb.	
	Fuel Bottles (2)	2.02 lb.	
	Valves (2)	.64 lb.	
	Pressure Regulator	.88 lb.	
	Fuel Lines	.60 lb.	
Generator			5.00 lb.
	Burner Head	.35 lb.	
	Burner Bullet	.57 lb.	
	Core & Pins	.51 lb.	
	T/E Modules	1.37 lb.	
	Cold Side Heat Exchanger	2.20 lb.	
Air System			2.90 lb.
	Generator Blower	.10 lb.	
	Generator Motor	.19 lb.	

Air System Cont'd.			
	Suit Blower	.33 lb.	
	Suit Motor	.32 lb.	
	Filter Case	.63 lb.	
	Inlet & Exit Plenums	.63 lb.	
	Air Temp. Adjustment	.70 lb.	
Packboard			1.09 lb.
External Wiring			.48 lb.
	Terminal Blocks	.14 lb.	
	Switches	.19 lb.	
	Wires	.15 lb.	
		TOTAL	15.21 lb.

Experimental Work

Experimental changes were confined to the generator burner system and to the power generator thermocouples. The other components of the unit were used as initially designed and fabricated.

a. Burner

The burner was tested as a separate piece of apparatus by substituting a thin stainless steel cylinder in place of the aluminum core used in the final assembly. This allowed operation of the burner at near design fuel rates with heat transfer away from the simulated core by natural convection and radiation to the atmosphere alone. Under these heat transfer conditions the core temperatures can and did go higher than the melting point of aluminum.

On initial operation the burner exhibited a high pitch screech. This screech was eliminated by drilling 4 rows of 8 equally spaced .056" diameter holes in the inner bullet just downstream of the burner head. These holes are just barely visible as black spots on the small end of the bullet in Fig. 7.

After these holes were introduced, the flame would sometimes flash back through the flameholder screen to the fuel port after 5 or 10 minutes of operation. Narrowing the annular gap covered by this flameholder screen by 1/32" and moving the fuel nozzle 1/8" towards the burner head eliminated this problem. That is it eliminated it providing the flameholder screen was firmly attached to the burner head so that no air could escape around this screen. Upon two occasions, spot welds holding this screen to the burner head pulled loose and flashback resulted. The screen was then arc-welded to the head and no further trouble of this sort has been experienced.

Much of the effort on the burner went towards smoothing out the heat transfer rates along the core. During this series of tests core temperatures were measured at 5 or 6 axial locations along the core and converted to heat flux rates assuming that substantially all the heat was lost by radiation with a core emittance of 0.8. Fuel flow to the burner was measured by measuring the time interval necessary to reduce fuel tank weight by a set amount, usually 30 gm. Air flow was not measured because accurate simple instrumentation interfered too much with the burner flow. It was estimated roughly on several occasions by measuring the total pressure of the air stream relative to ambient at one point in the inlet of air tube to the burner. This flow was of the order of 0.8 CFM.

As initially tested the burner core had a pronounced hot band 1" to 2" downstream of the burner head. Heat flux rates at this 1" to 2" location, at a fuel rate of 0.18 lb/hr, were in excess of 14,000 BTU/hr/ft^2 and dropped to 1,700 BTU/hr/ft^2 6-1/2" downstream of the burner head. The desired rates were 8,400 BTU/hr/ft^2 at this 1" to 2" location down to 6,400 BTU/hr/ft^2 at the 6-1/2" location. After the four rows of 0.056" dia. holes were drilled in the bullet to eliminate the screech, the heat flux rate at the 1" to 2" location dropped to 12,500 BTU/hr/ft^2 and increased to 3,200 BTU/hr/ft^2 at the 6-1/2" location. An additional row of holes gave little or no improvement.

To further reduce the heat flux variance along the core a series of screens, both cylindrical screens mounted co-axially with the bullet and longitudinal strips extending radially from the bullet were tried. In general, a screen either cylindrical or longitudinal at any lengthwise location reduced the core temperature at that location and increased it at unscreened locations. An exception to this was a screen wound tightly over the bullet at its maximum cross-section at the exhaust end of the burner. This apparently gave a slight improvement in heat flux distribution and was included in the final assembly. A marked beneficial change resulted from placing a screen tightly against the core and extending along the core from 1/2" to 3-1/2" downstream of the burner head. This substantially reduced the heat flux through the 1" to 2" location. This screen was also included in the final generator assembly. With the addition of these two screens, at a fuel rate of 0.18 lb/hr., the heat flux in the 1" to 2" location was 9,000 BTU/hr/ft^2 and 4,100 BTU/hr/ft^2 at the 6-1/2" location. After the addition of the 'core' screen in the upstream

end, work on the burner separate from the generator was dropped. It was felt that the substitution of the higher thermal conductivity would further improve the heat flux distribution to an acceptable if not ideal level. This turned out to be the case.

b. Thermocouples

Because of a substantial amount of reasonably successful experience with them, we selected 'N' type lead telluride and 'P' type germanium bismuth telluride as the thermoelectric materials. We had previously fabricated and constructed thermocouples of these materials using Armco Iron caps and straps joined by procedures similar to those given in Section 5 in a size suitable for this application. An individual couple so constructed had given 3000 to 4000 hours life to 20-25% degradation, with many cycles, when tested in a argon-hydrogen atmosphere. Other individual couples had given 1000 to 2000 hours life to the same 20-25% degradation, with many cycles, when tested in an air atmosphere.

There are obvious advantages in generator construction and weight if the couples do not have to be sealed into an artificial atmosphere. Therefore, an unsealed design was decided upon with an attempt to be made to improve the operating life of the thermocouples by substituting stainless steel clad copper for the iron straps and caps. During testing in an air atmosphere the soft iron is corroded quite badly, particularly at the hot side joints with the thermoelectric legs. Stainless clad copper was used because the electrical resistance of solid stainless steel would have been too high using the thin strap indicated by stress considerations.

This substitution of the stainless clad for iron was completely successful as far as joining the 'N' legs of couples was concerned. Fabrication

yield with the 'P' legs was 10% or less, however. After a number of trys using modifications of the initial joining process failed to improve this yield, the attempt to use stainless clad copper straps and caps was abandone.

The couples for the generator were then made up using Armco Iron.

Two modules of four couples each were assembled and put on life test. The first module used couples which were already available from previous work. The second module couples were selected at random from those made for the generator. The couples of the first and second module were fabricated using what is thought to be identical processes. The geometry of the couples was the same except that in the first module the straps and caps were 1/16" thick and the legs were on 7/16" centers, whereas in the second modules, the couple straps and caps were 1/32" thick, and the legs were on 3/8" centers. The thinner straps should substantially reduce thermal cycling stresses. The 'N' leg material was the same except for accidental batch variations between lead telluride of good quality. The 'P' leg material in the first module was 93% germanium telluride, 7% bismuth telluride while it was 95% germanium telluride, 5% bismuth telluride in the second. It is the writers opinion that the 95-05 'P' material makes for better couples in this size of couple.

The first module was tested in an argon-hydrogen atmosphere at approximately 450°C hot strap temperature and 110°C cold cap temperature. This module was thermally cycled from room temperature to operating temperature about once every 100 hours.

The second module was tested in an air atmosphere at approximately 450°C hot strap temperature and 125°C cold cap temperature. This module was thermally cycled from room temperature to operating temperatures every 8 hours. Approximately 6 of the 8 hours was at operating temperatures.

The results of these life tests are given in Fig. 8. This is a plot of module power output as a function of hours on test. Since the two modules were not run at the same temperature differences between hot and cold sides, both sets of data were referred to a 330°C temperature difference by assuming that the power of the module varies as the square of the temperature difference. This is accurate within 2 or 3% for the test conditions and couples involved.

As can be seen in Fig. 8, the initial output of the second module (Module #2) was substantially better than that of the first (Module #1). The rapid initial fall off in power output of both modules is probably caused by a phase change in the 'P' material that takes place as it ages during operation.

Subsequent degradation is probably a result of cracks from thermal stress and atmospheric corrosion. It is apparent that Module #2 is degrading more rapidly than did Module #1. Module #2 is ungoing frequent thermal cycling and is open to atmospheric corrosion. Even so it still enjoys a substantial power advantage over Module #1 at 1500 hours on test. It is anticipated that the thermoelectric modules of the generator will be replaced at 1500 hours during major overhaul.

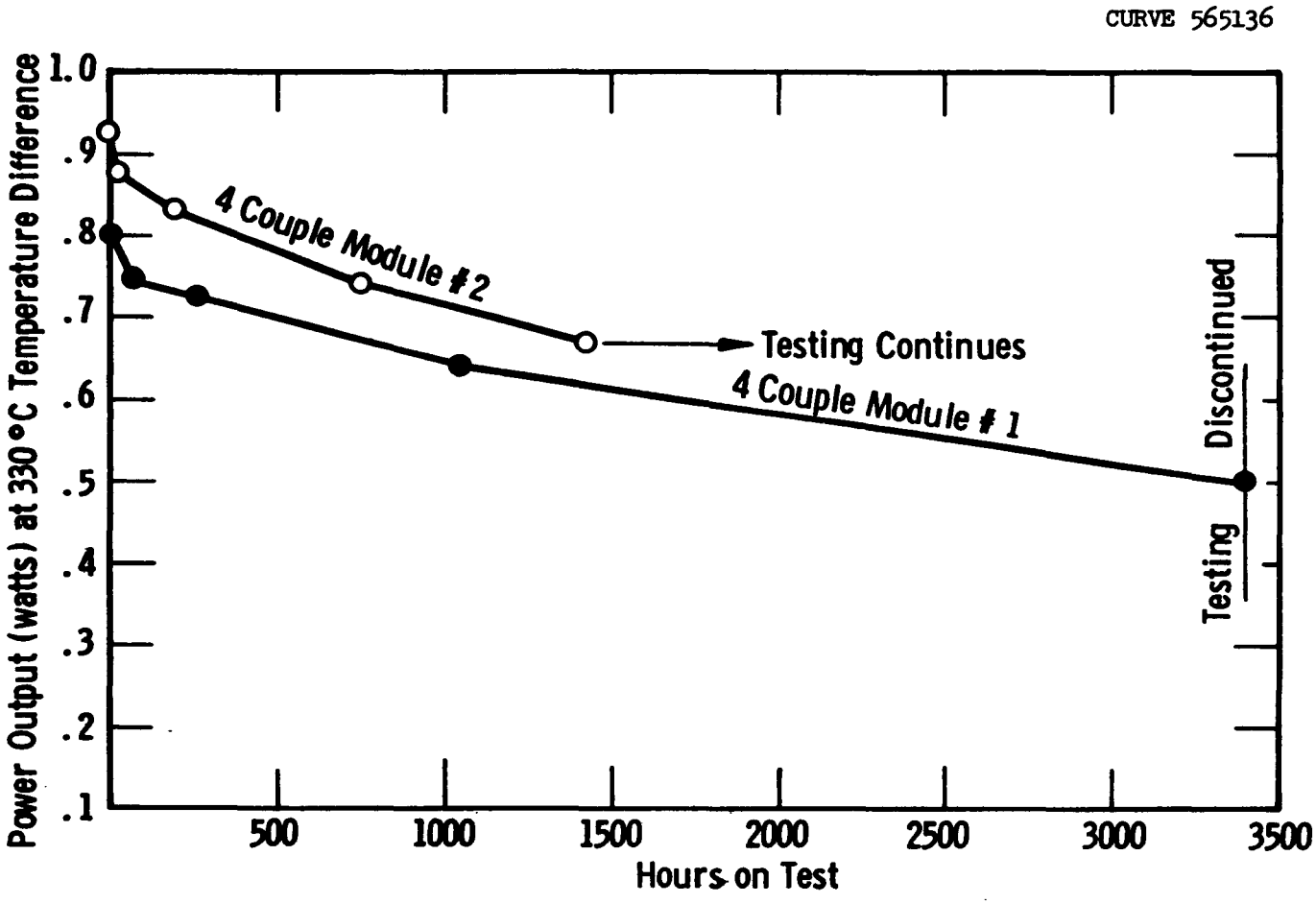

Fig. 8—P-316 Thermocouple Module Tests

Performance Test of Unit

Prior to delivery of the unit to the U. S. Army Natick Laboratories, the unit was run 14 times with a total accumulated operating time of 10.25 hours. Most of these runs were for the purpose of checking out or demonstrating the operating capability of the unit. In addition 4 runs were made in attempt to improve the hot side temperature distribution along the length of the generator by changing burner screening arrangements. As has been remarked before, this temperature or heat flux distribution is acceptable but not ideal. No improvement resulted from these runs.

a. Instrumentation

Temperature measurement was by 28 ga. chromel-alumel thermocouple wire read on a Leeds-Northrup potentiometer. For measurement of hot core and hot strap temperatures, the thermocouple was peened into the part to be measured. For measurement of cold cap and casing temperatures, the thermocouple was soldered to the respective part. Air temperatures were measured by single bar wire couples inserted with approximately 1 inch of lead parallel to the flow direction.

The location of the various thermocouples in the generator is shown by Fig. 9. This depicts the modules of the generator as through they had been peeled from the core by slitting the skin at the top of the generator and opening them to either side onto a plane surface. This figure also shows the series electrical hookup of the generator modules, starting with #1 and continuing through #20. It should be noted that modules #5 and #6 and #15 and #16 are physically side by side in the generator.

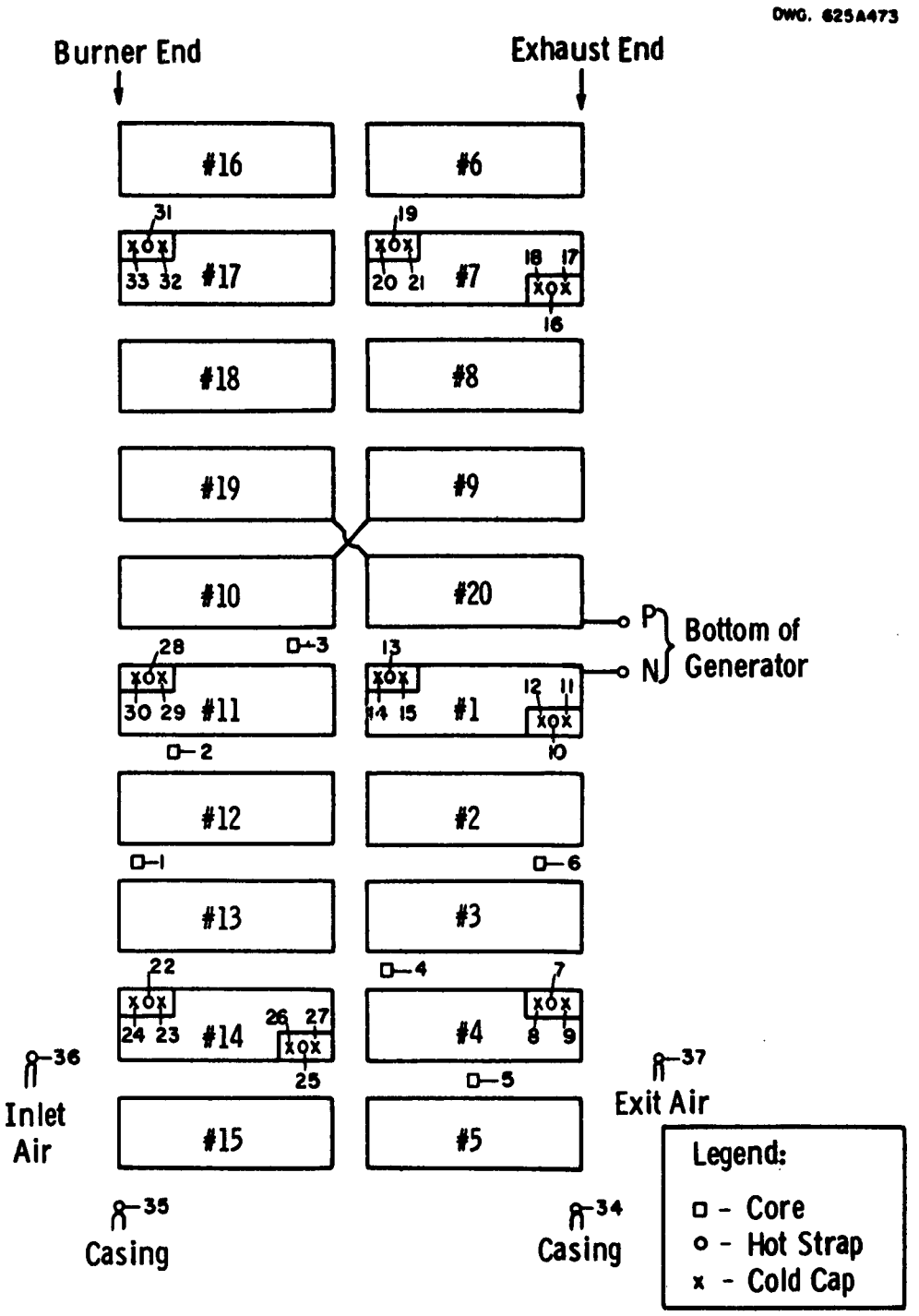

Fig. 9—Temperature measurement locations

Air flow and static pressure available for suit use was measured by a metering section attached to the suit blower exit. This section consisting of a transition piece 1-1/2" long from the suit blower to an 8" length of 1-1/2" O. D., 1049 wall tubing. The tubing exhausted to ambient through a sharp edged orifice 5/8" in diameter. Two static taps were located 1-1/2" upstream os this orifice on opposite sides of the tube.

A rough estimate of generator cooling air flow was obtained by measuring a static pressure at the generator blower exit. This number could be used in conjunction with measured generator blower rpm and the blower characteristics to estimate this airflow. In addition a 'Volometer' traverse was run at the cold side heat exchanger exit on one occasion.

The rpm's of both blowers were measured by a 'Strobotac'. Electrical potential and current were measured by appropriate Westinghouse d.c. voltmeters and ammeters. Fuel flow was measured by a weighing procedure as previously described under burner development.

b. Performance

Measurements of the units's performance are given in Table I which follows:

Table I

Unit Performance

Reading Number	12	13	16	17	18
Ambient Temperature (°F)	75°F	75°F	77°F	39°F	110°F
Ambient Pressure ("Hg)	28.6	28.6	28.8	28.8	28.8
Suit Blower Flow (CFM)	11.7	11.3	11.3	11.3	11.2
Suit Blower Δ P ("H_2O)	4.62	4.37	4.25	4.55	4.0
Suit Blower Δ P ("H_2O) at 12 CFM Flow (calculated)	4.50	4.11	4.00	4.30	3.74
System Electrical Requirements					
EMF (Volt)	10.85	10.4	10.35	10.3	10.1
Current (amp)	2.55	2.4	2.45	2.55	2.3
Power (Watt)	27.6	25.0	25.0	26.2	23.2
Generator Output to a Matched Load					
EMF (Volt)	8.50	8.20	-	-	-
Current (amp)	3.55	3.30	-	-	-
Power (Watt)	30.0	27.0	-	-	-
Generator Fuel Flow (lb/hr)	0.26	0.23	0.24	0.25	0.23

Readings 12 and 13 were taken using a full set of instrumentation as previously described. Aside from the obvious value of taking this data, these readings were used to set the fuel pressure regulator so that the unit would put out, approximately, the contractural goal of 12 CFM at 4" H_2O static pressure from the suit blower.

Readings 16, 17, and 18 were checks of the effect of different ambient temperatures on the unit's performance prior to shipment to the U. S. Army's Natick Laboratories. All except three of the temperature measuring thermocouples internal to the generator had been cut off to make a neat package prior to these runs. The only couples left in were those recording the highest temperatures for 'hot' spot monitoring. As can be seen, unit output increases as ambient temperature decreases.

Referring to Table I, there are two sets of suit blower static pressures (ΔP) given. The upper or first one is the actual value of ΔP as measured using the 5/8" diameter sharp edged orifice and the flow values just above are those actually measured at this measured ΔP. The second value of ΔP is the value that calculation says would have been obtained had the orifice on each of these readings been sized to give exactly 12 CFM suit blower flow. The calculation assumes that the unit's component efficiencies do not change during the small amount of extrapolation involved.

For readings 12 and 13 there are two sets of electrical performance numbers given. The first set is the result of running the unit in its intended configuration with the two blower motors as the generator load. The second set is the result of substituting a variable resistance for the suit blower motor so that the external or load impedance could be matched to the generator internal impedance (condition of maximum generator power output). As can be seen, there is more power available in the generator than can be utilized by the unit because of some mismatch between components of the unit. The difference in output between readings 12 and 13 is a result of lowering the fuel flow to the generator from readings 12 to 13. The differences in output between

readings 13 and 16 are unexplained as is the difference in measured fuel flow rate. That the readings were taken during different runs on different days is no explanation since the fuel pressure and ambient conditions were almost identical for each reading. The differences between these two runs may be taken as an indication of the reproducibility of results.

The individual temperatures as measured during Reading #12 are plotted as a function of lengthwise position in Fig. 10. It will be noted that there was little spread in hot strap temperatures at any axial location but a decided slope in these temperatures from end to end. The wide spread in temperatures on the thermocouples cold side is largely a result of tilted cold caps on some of the thermocouples as fabricated. A tilt of .001" from side to side or end to end will cause an increase of cold cap temperatures of about 40 or 50°C over one which is flat.

The averaged temperatures from Reading #12 are compared to design intentions as a function of lengthwise position in Fig. 11. Also noted in this figure are the measured generator outputs and inputs as compared to the design conditions. Values for the cold side heat exchanger pressure drop and cooling flow are not included in this figure. The design values were 0.75" H_2O and 18 CFM. The measured values were 24 CFM and 0.38" H_2O.

As can be seen matched power output was 10% below design value at a fuel flow 8% greater than design. A small part of this lower performance is because the design conditions are more favorable to the generator than the actual operating conditions of Reading #12. Most of it, however, is caused by the sloping temperature along the core on the hot side. It should be remarked that the design conditions are ideal conditions and unlikely of

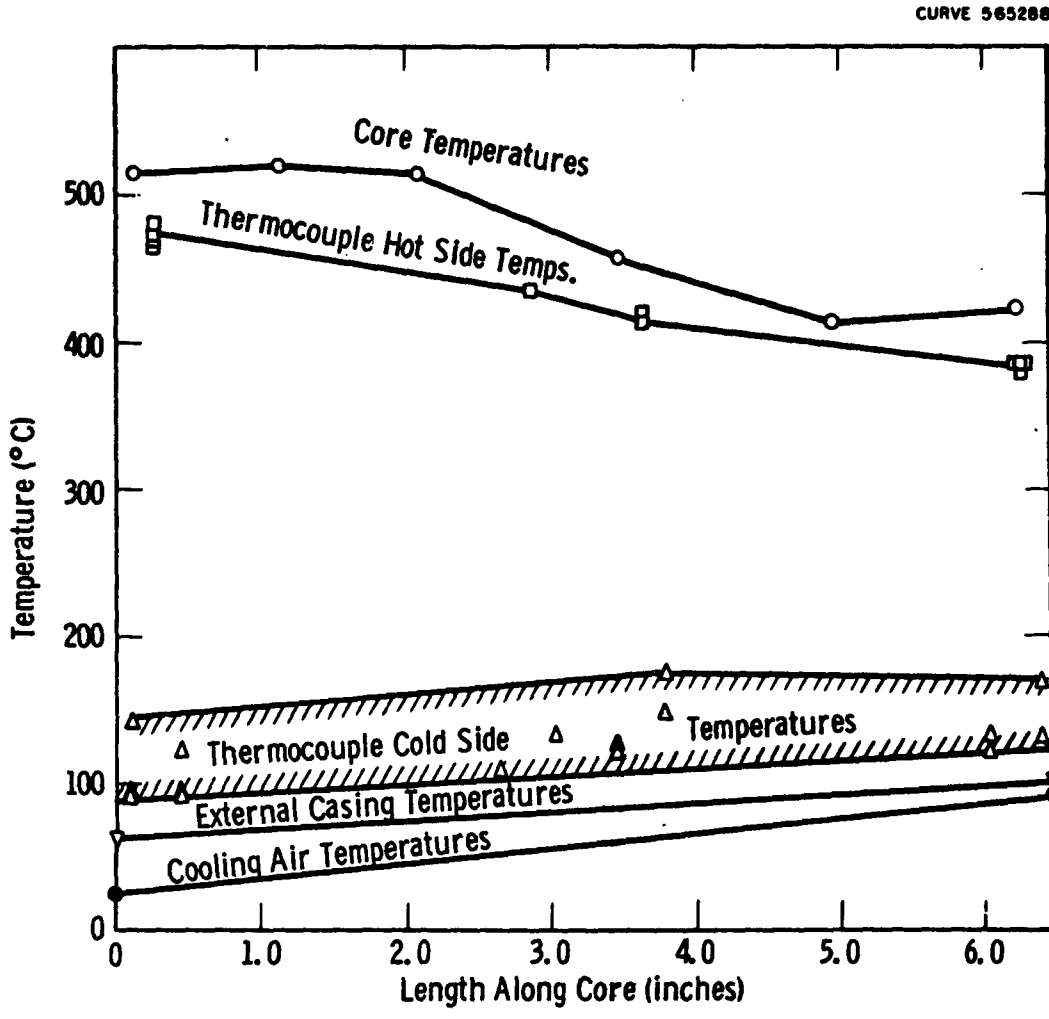

Fig. 10—Measured temperatures in generator (Run #12)

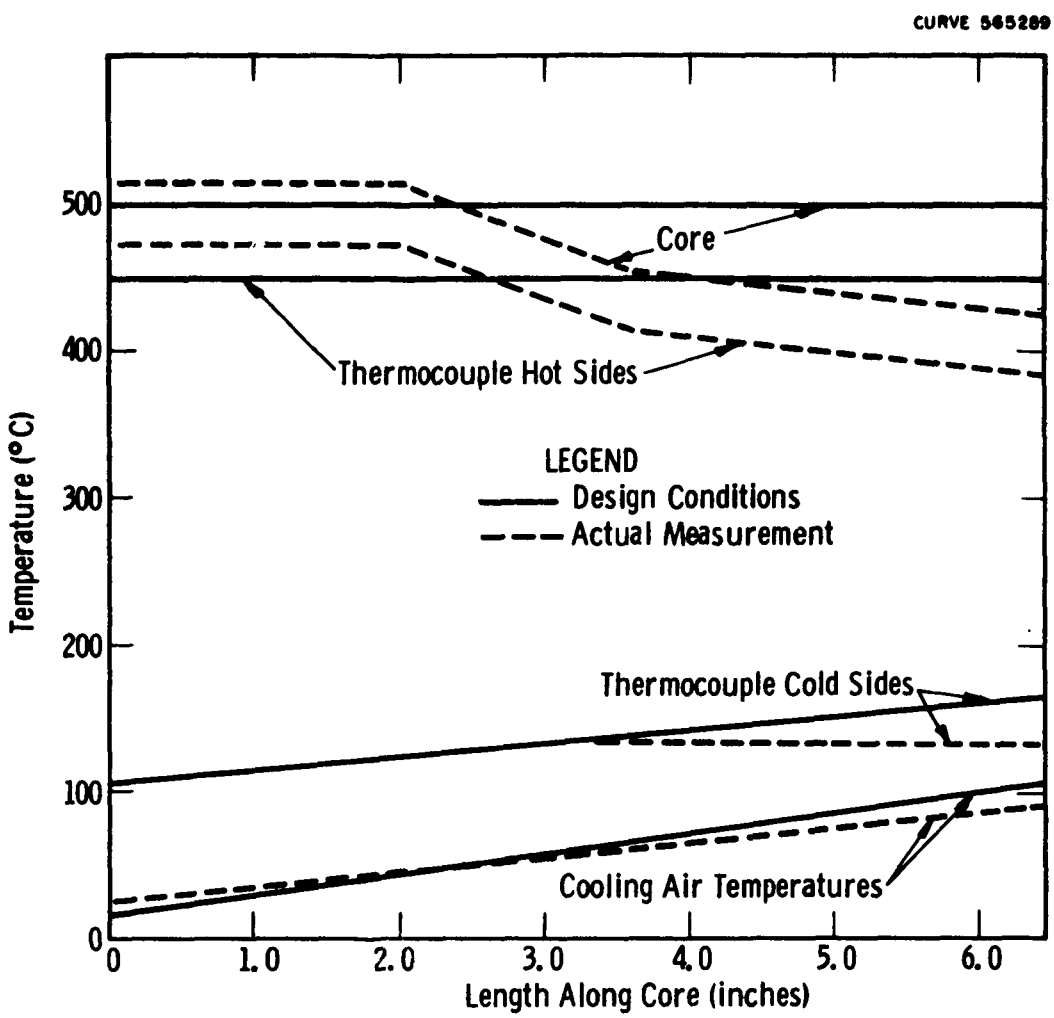

	Run #12	Design Conditions
Current	3.54 amp	3.63 amp
E.M.F. matched	8.5 volt	9.1 volt
Power	30 watts	33 watts
Couple $\Delta T_{average}$	301°C	314°C
Ambient Temp.	24°C	15°C
Ambient Press.	0.96 atmos.	1.0 atmos.
Fuel Flow	0.26 lb/hr	0.24 lb/hr

Fig. 11—Comparison: Design conditions vs. actual generator (Run #12)

complete attainment.

Conclusion

It is apparent that the performance level of this unit is in excess of the requirements as set forth under Phase I of the Contract and paraphrased in the Introduction of this report.

Perhaps an even better illustration of a substantial step forward is to compare the present unit's performance with that of a Silvercel battery powered unit previously delivered for the same duty.

	Battery Unit	Thermoelectric Unit
Useful Flow	10 CFM @ 2.5" H_2O	12 CFM @ 4" H_2O
Fully Fueled Weight	18 lb.	15.25 lb.

While this unit is a successful one within the intent of Phase I of the Contract, substantial further improvements can be made. For example, only about 80% of the potential power of the unit is being developed and utilized. The weight of the unit can be substantially reduced, as anticipated in Phase III of the Contract, by substituting aluminum for brass and steel in the fuel valving and piping. Use of liquid fuels such as gasoline will also reduce weight by eliminating the need for heavy walled L. P. fuel storage containers. Use of liquid fuels will also simplify problems of field fuel supply.

The rate of degradation of the lead telluride, germanium bismuth telluride thermocouples used in this generator, while probably tolerable (based on module life tests) for a major overhaul period of 1500 hours, is disappointing. This deficiency can be substantially corrected by use of the new antimony bismuth telluride materials in future generators. These materials have shown very little

or no degradation over life testing periods of interest to this application (3000 hours) when well sealed or protected from the earth's atmosphere. Sealing of the thermocouples against the atmosphere will also eliminate any possibility of systemic pickup by persons using the unit of thermoelectric material such as tellurium.

Research Memo 62-129-243-M1 July 10, 1962

DETERMINATION OF THE FIGURE OF MERIT OF THERMOELECTRIC MATERIALS

R. C. Miller and R. W. Ure, Jr.

The efficiency of a thermoelectric generator depends on the properties of the material through a single parameter, TZ, the figure of merit, which is defined as

$$TZ = \frac{T\alpha^2}{\rho\kappa}$$

where T is the absolute temperature, α the Seebeck coefficient, ρ the electrical resistivity, and κ the thermal conductivity. There are two basically different approaches to the determination of the figure of merit. These are:

(1) To separately measure the individual parameters α, ρ, and κ and to compute TZ.

(2) To directly determine TZ from a measure of the heating or cooling at the ends of a sample by the Peltier effect.

The second approach would appear to be the preferable. However, at least as much care must be taken to eliminate heat leaks as in the separate determination of parameters and since the values of the individual parameters are often of as much importance as TZ, the first approach is preferable. The method of small area contacts, which will be discussed in more detail later, does avoid some of the problems associated with heat leaks but introduces additional problems in the form of uncertain contacts and for this reason is also less desirable than the separate determination of parameters.

In the following sections, we will discuss: (1) the method of measuring the individual parameters α, σ, and κ and some of the possible errors that enter into the determination of these quantities, and (2) some of the methods of determining TZ directly, in particular the Z meter, and the method of small area contacts and the errors entering into these determinations.

Before discussing the measurements, it should be emphasized that it is almost always advisable to investigate the phase relationships of a material before performing any extensive series of measurements on the material. For example, a large number of measurements have been performed on $AgSbTe_2$. However, this material is reported to be only truly stable in the temperature range 340°C to 575°C. Below 340°C, it decomposes into Ag_2Te and another phase which is related to Sb_2Te_3. This decomposition is rather slow and, by rapid cooling below 340°C, $AgSbTe_2$ can be gotten as a metastable phase at room temperature. The material actually is not $AgSbTe_2$ but a ternary compound of nearly that composition and a small (~5-15%) amount of a second phase is metastable, measurements can be performed at room temperature and, if performed rapidly, at temperatures approaching 340°C. Above this temperature and below 575°C, the material is stable and there is no difficulty in performing the measurements. If this material were now incorporated in a thermoelectric generator where part of the material was held at a temperature in the range of 200-340°C for a long period of time, the material would decompose and the measurements made on the metastable phase would be of no significance in predicting the long term performance of the generator.

In any measurement of the bulk properties of a solid in which high accuracy is desired, it is necessary to have samples which are homogeneous and free from cracks, holes, or other macroscopic imperfections. If the crystal structure of the material is anisotropic, some attention must be paid to the crystal orientation of the sample being measured.

I. INDIVIDUAL PARAMETERS

Electrical Resistivity

The usual procedure for measuring the resistivity consists of passing a known current I through a uniform bar of the material and measuring the voltage drop E between two probes, Fig. I. If the distance between the

probes is ℓ, the cross-sectional area is A, and the current in this region

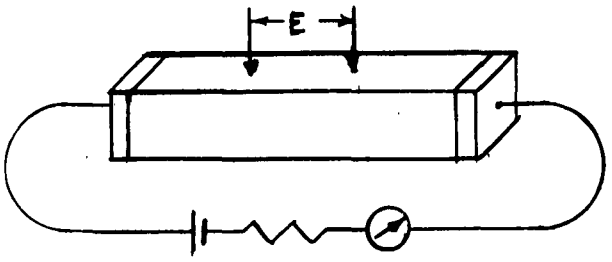

Fig. I

is uniform, the resistivity is given by expression

$$\rho = \frac{E}{I} \cdot \frac{A}{\ell} \qquad (1)$$

In the range of resistivities usually encountered in thermoelectric materials (10^{-2} - 10^{-4} ohm-cm), there are only two likely sources of error. These are:

(1) Seebeck emf's Produced by Temperature Gradients in the Sample

If there is a temperature gradient in the sample then the two voltage probes and the sample form a thermocouple and the resulting Seebeck emf will be added onto the voltage E. The usual procedure for eliminating these stray emf's is to simply reverse the current and average the two voltages. However, in a good thermoelectric material with a steady current flowing, the Peltier effect at the ends of the bar produces a temperature gradient which reverses direction when the current is reversed. The Seebeck emf developed because of this temperature gradient is not necessarily eliminated by reversing the current and averaging the voltages. This particular effect is the basis of the operation of the Z meter which will be described later. The methods of eliminating this error are based on the fact that a certain length of time is required to establish the temperature gradient in the material after a change in the current flowing. One solution is to use an AC current of such a frequency (> 10 c.p.s.) that the current reverses itself many times during the period of time required to establish

the temperature gradient. Another solution is to use contacts of large heat capacity at the ends of the sample. This increases the length of time required to establish the temperature gradient. Then by simply reversing a DC current and measuring the voltage rapidly, this error can be eliminated.

(2) Non-Uniform Current Distribution in the Sample Due to Poor End Contacts

If the current distribution in the sample is non-uniform, the resistivity calculated from Eq. (1) will be in error. If the probes are placed at least one diameter from the ends of the sample, the current will be reasonably uniform at the probes regardless of the nature of the contact at the ends of the sample. For short samples, it is usually necessary to tin the ends of the sample and solder copper contacts to the sample to insure a uniform current distribution.

The only additional precaution required to permit measurement at high temperature is to choose insulation materials whose resistivities are large compared to that of the sample at the operating temperature. Boron nitride, mullite, and alumina are generally satisfactory.

For samples which can be cut so that their length is larger than 5 to 10 times their width or thickness, the electrical resistivity can be measured to an accuracy of $\pm 3\%$ easily and to $\pm 1\%$ with some care.

Seebeck Coefficient

The Seebeck coefficient is determined by measuring the difference in voltage ΔV and the difference in temperature $\Delta T = T_1 - T_2$ between the same two points on a sample in which there is a small temperature gradient. It should be emphasized that the Seebeck coefficient of a homogeneous material is independent of the exact nature of the temperature gradients in the material and depends only on the temperature difference between the two points at which ΔV is measured. If ΔT is such that $(\Delta T/T_1)^2$ is small compared to unity, the relative Seebeck coefficient is given by the expression

$$\alpha = \frac{\Delta V}{\Delta T}$$

The absolute Seebeck coefficient of the sample is obtained from the relative Seebeck coefficient by subtraction of the absolute Seebeck coefficient of the lead wires

$$\alpha_{abs}(\text{sample}) = \alpha_r - \alpha_{abs}(\text{leads})$$

Two practical arrangements for the measurement of the Seebeck coefficient are shown in Figs. 2a and 2b. In both these arrangements, the sample is

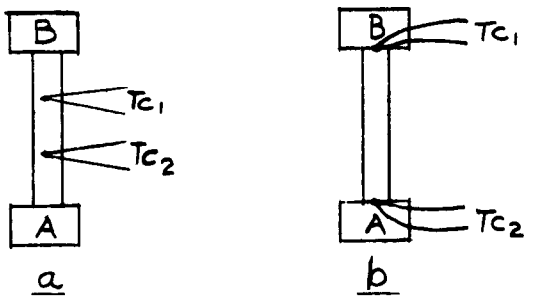

Fig. 2

held between two metal blocks A and B and a heater in the upper block B produces a temperature gradient in the sample. In the arrangement in Fig. 2a, the temperature difference is measured by means of the two thermocouples Tc_1 and Tc_2 which are in good thermal and electrical contact with the sample. The voltage difference is measured between the similar leads of the two thermocouples, (e.g., if copper-constant thermocouples were used, the voltage would be measured between the two copper leads and the Seebeck coefficient determined would be relative to copper). The arrangement in 2b differs only in that the two thermocouples are fastened to the metal blocks. This arrangement is more convenient and is as satisfactory as 2a provided the blocks make good thermal and electrical contact to the sample.

For the usual range of electrical resistivity encountered in thermoelectric materials, there are only two likely sources of error. These are:

(1) Poor thermal contact between sample and thermocouple

Let us consider first the arrangement shown in Fig. 3.

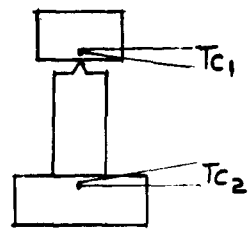

Fig. 3

The small irregularity on top of the sample is the only part of the sample in thermal and electrical contact with the upper block. Since all of the heat that flows through the sample must pass through this irregularity and its cross-sectional area is small compared to that of the rest of the sample, most of the temperature drop will occur in this irregularity. If the composition of this small region is the same as the rest of the sample, the ratio of the measurements ΔV and ΔT will be the correct Seebeck coefficient. However, if its composition is different, then the measured Seebeck coefficient can be quite different from the correct value.

This error can be avoided by using the approach of Fig. 2a. If the thermocouples are in good thermal and electrical contact with the samples and fine wires are used for the thermocouples so as to minimize the amount of heat conducted down the leads, then there are no large thermal gradients in the vicinity of the thermocouple and the correct Seebeck coefficient will be measured. Unfortunately, this arrangement cannot always be used for the following reasons. First, it is difficult to secure good thermal contact between the thermocouple and sample by simply inserting the thermocouple in a hole in the sample. Second, many of the thermoelectric materials react with the thermocouples. To avoid a change in calibration of the thermocouples due to the reaction, some kind of jacketing must be used on the thermocouples. The jacketed thermocouples have relatively large thermal conductivities and conduct large amounts of heat from the sample giving large thermal gradients in the sample in the vicinity of the contact.

The arrangement of Fig. 2b is greatly more satisfactory. The jacketed thermocouples can be bolted into the metal blocks insuring good thermal contact. For thermoelectric materials having thermal conductivity less than .25 watt/cm/°C and a length of 2 cm or more, lapping the ends of the sample and filling the apparatus with hydrogen or helium gas is sufficient to reduce the temperature drops associated with the contact to a negligible fraction of the total drop across the sample.

(2) Errors in thermocouple calibration

There are two kinds of errors that can arise because of poor calibration of the thermocouples. The first is due to slight differences between the two thermocouples. In this case, the temperature will be accurate, but the difference in temperature ΔT will be in error. This error is easily eliminated by simply measuring ΔV and ΔT at two or more different temperature gradients and plotting ΔV vs ΔT(observed). If there is no difference between the thermocouples, the line will pass through the point $\Delta T = 0$, $\Delta V = 0$. If the line does not pass through this point, the Seebeck coefficient can be calculated from the slope of the line.

The second error is much harder to detect, and it arises when the calibration of both thermocouples are the same and wrong. This can easily happen, for example, if exposed chromel-alumel thermocouples are used to measure the Seebeck coefficient of tellurides at high temperatures. After several hours operation at temperatures above 500°C, the calibration changes such that the measured Seebeck coefficient is ~30% higher than the true value. The only ways to avoid this error are to use jacketed thermocouples and to frequently check known samples to detect deterioration of the thermocouple calibration.

The only additional precaution needed to permit measurements at high temperature is to be certain that the electrical resistivity of the insulating material is large compared to that of the sample. When the precautions outlined above are taken, the Seebeck coefficient can be measured with an accuracy of the order of $\pm 2\%$ to $\pm 4\%$.

Thermal Conductivity

Basically, the methods of measuring the thermal conductivity and the electrical resistivity are similar. In the case of the electrical resistivity, a given electrical current is passed through the sample and a voltage drop measured, while for the case of the thermal conductivity, a known thermal current is produced in the sample and a temperature drop determined. A simplified apparatus is shown in Fig. 4. It consists of a heat source, in

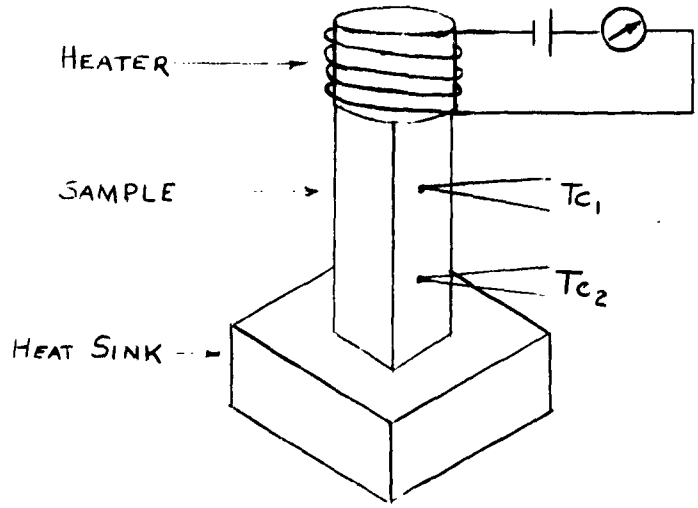

Fig. 4

this case a known resistor and a means of passing a known current I through the resistor, a heat sink which is simply a block of material having sufficient heat capacity so that its temperature does not change significantly during the course of the measurement, and the two thermocouples to measure the temperature drop, ΔT. If the thermocouples are a distance ℓ apart, the cross-sectional area is A and the heat flow uniform, the thermal conductivity is given by the expression

$$\kappa = \frac{I^2 R}{\Delta T} \cdot \frac{\ell}{A}$$

In practice, it is much more difficult to measure the thermal conductivity than the electrical resistivity. The reason is simply that other than a vacuum at low temperatures ($< 100^{\circ}K$), there are no good thermal insulators.

It is an easy matter to find electrical insulation whose resistance is 10^8 times that of the thermoelectric materials being measured while at moderate temperatures (~300°K), the thermal conductivity of the materials used for thermal insulation is only a 1/100 to a 1/10 that of most of the common thermoelectric materials. Thus in the measurement of electrical resistivity all of the current from the battery passes through the sample. In the measurement of thermal conductivity unless elaborate precautions are taken, only a fraction of the heat generated in the heat source passes through the sample, the remainder being lost through various heat leaks.

There are two practical arrangements for the measurement of the thermal conductivity. The first is the absolute method shown in Fig. 4 in which the amount of heat flowing through the sample is calculated from the electrical power dissipated in the heater. The second is the comparative method shown in Fig. 5. In this apparatus, the sample and a standard material

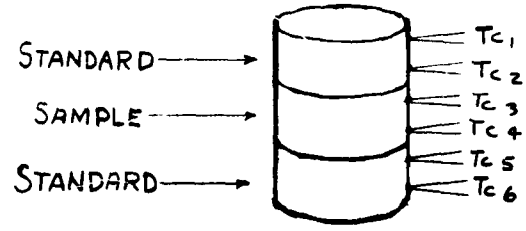

Fig. 5

are arranged so the same amount of heat passes through both materials. The thermal conductivity of the sample is then given by the equation

$$\kappa_{sample} = \kappa_{std.} \cdot \frac{\Delta T_{sample}\, \ell_{std.}}{\Delta T_{std} \cdot \ell_{sample}}$$

The likely sources of error in the measurement of thermal conductivity are:

(1) Heat leaks: As mentioned above, the problem of heat leaks is very serious in the determination of the thermal conductivity. There are two general approaches to minimize the heat leaks. The first is to use short fat

samples. In this way, the ratio of the total heat conduction through the sample to that lost at the edges is increased and the accuracy improved. This method is generally used in a comparative apparatus because the only heat leaks that effect the accuracy of the result are those from the sides of the sample and standards. However, when the samples are short, it becomes difficult to accurately define the distance between the thermocouples since the diameter of the thermocouples becomes a significant fraction of the specimen length. In the absolute apparatus, one also has to prevent heat leaks from the heat source and thermal guarding must be used. This consists of placing a shield around the sample and heater and matching the temperature at every point on this shield to that of the sample or heater at the closest point. If the temperatures were matched perfectly and the shield was a small fraction of the diameter of the sample away from the sample, the heat leaks would be completely eliminated. In a practical arrangement using modest sized sample 1/2" long x 1/2" dia., the heat leaks amount to 10% of the total flow at 200°C and increase roughly as T^3.

(2) Non-uniform temperature gradients in samples due to poor end contact: This error arises in the same fashion as described under the measurement of electrical resistivity. Eliminating it is somewhat more difficult since short fat samples are required to minimize heat leaks. The best solution is to solder the sample to the heater and the heat sink. The next best solution is to carefully lap the ends of the sample and the matching surfaces of the heater and heat sink, and to fill the apparatus with a gas having a high thermal conductivity, preferably either with H_2 or He.

(3) Errors in thermocouple calibration: This problem and its solution is exactly the same as in the case of the measurement of the Seebeck coefficient.

The extension of thermal conductivity measurements to high temperature is very difficult. If a vacuum is used as thermal insulation, the heat leaks due to radiation increase as T^3 and are usually of the same order of magnitude as the heat conduction through the sample by 300°C. For high temperatures, it is preferable to use an opaque solid material as the insulator and to use samples of large A/ℓ to minimize the heat leaks.

When the heat leak due to radiation is small compared to the heat flow along the sample, one can correct the results for this heat loss. However, there are several uncertainties in this correction which will introduce large errors in the result of this correction is large. The correction depends on the emissivities of the sample and the apparatus. The emissivity of a material depends on the condition of the surface of the material and can change by large factors if the surface is changed, for example, by oxidation. Thus the emissivity of a given piece may change with time and therefore there is an uncertainty in the emissivity at the time the measurements are made. Since the correction depends in a different way on the emissivity of the sample, the apparatus, and in some cases the sample contact materials, one cannot get an accurate correction by measuring the average emissivity at the time the measurement is made.

Another possible solution is to use a sample geometry in which the heater is completely surrounded by the sample. However, this requires considerable effort in the preparation of each sample to be measured.

Diffusivity

Because of the difficulties involved in the direct measurement of the thermal conductivity, the measurement of the diffusivity has been proposed as an alternate method of determining the thermal conductivity. The diffusivity D is related to the thermal conductivity by the equation

$$D = \kappa/C,$$

where C is the specific heat per unit volume. The apparatus for the measurement of the diffusivity (Fig. 6) consists of a sample of constant uniform

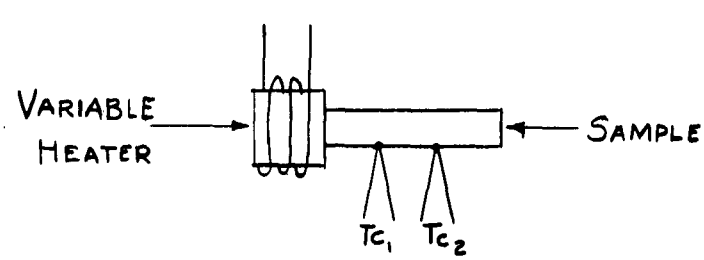

Fig. 6

cross-section, with a heater attached to one end and provisions for the measurement of the temperature at two or more points along the bar. The apparatus is placed in an evacuated container which is maintained at a constant temperature T. The power input to the heater is varied in such a manner that the temperature at the end of the sample varies sinusoidally with time. The amplitude of the temperature variation is small compared to T. Under these conditions, a temperature wave will be propagated along the bar. The two thermocouples permit the measurement of the phase velocity V of the wave and the attention of the wave as it passes along the bar. The attenuation is expressed in terms of the logarithmic decrement per unit length δ and is given by the expression

$$\delta = \frac{\ln T_1/T_2}{\ell}$$

where T_1 and T_2 are the amplitude of the wave at the two thermocouples and ℓ is the distance between thermocouples.

If there are no heat leaks to the surroundings the diffusivity can be calculated from a single measure of either δ or v by the equations

$$\delta = (\omega/2D)^{1/2}$$

and

$$v = (2\omega D)^{1/2}$$

where ω is the angular frequency of the temperature variation. If one assumes that the only heat leaks are those due to radiation, we have

$$\delta = \left\{ \left[a^4 + \left(\frac{\omega}{2D}\right)^2 \right]^{1/2} + a^2 \right\}^{1/2}$$

and

$$v = \frac{\omega}{\left\{ \left[a^4 + \left(\frac{\omega}{2D}\right)^2 \right]^{1/2} - a^2 \right\}^{1/2}}$$

where

$$a = \beta \cdot \left(\frac{\epsilon T^3}{CD}\right)^{1/2},$$

β is a constant dependent on the shape of the sample, and ϵ is the emissivity of the sample. In the presence of heat leaks, it is no longer possible to determine D from a single measurement and it is necessary to measure either v or δ at two or more frequencies, or to measure both v and δ at a single frequency. In the later case, D is given by the simple expression

$$D = v/2\sigma$$

There are several practical difficulties in the measurement of diffusivity. Firstly, for materials of small diffusivity, the attenuation is large and the amplitude of the temperatures wave decreases rapidly with distance. Under these conditions, it is difficult to measure v and δ accurately. Secondly, at higher temperatures, the parameter a becomes important and the attenuation increases rapidly within increasing temperature. The decrease in accuracy accompanying this increase actually sets an upper limit to the temperature at which measurements can be made. Third, since the measurements are performed in vacuum, it is suitable only for those materials that have very low vapor pressures. If a gas is admitted to the apparatus to prevent volatilization or decomposition of the sample, the equations given for δ and v are not applicable. It might be possible to derive new expressions for special cases. However, because of the possibility of convection and the heat capacity of the gas or any material placed in contact with the sample to prevent convection, the expression would be complicated. The final difficulty is that the specific heat at constant pressure C must be measured in order to obtain the thermal conductivity from the diffusivity. This specific heat can be estimated theoretically, but this may introduce an appreciable error.

The thermal conductivity measurement is the most difficult measurement which enters into the calculation of the figure of merit. At temperatures in the vicinity of room temperature and below, the thermal conductivity can be measured to an accuracy of $\pm 3\%$ in a reasonable length of time. The accuracy of this measurement has been established by comparisons of the measured performance of a thermoelectric couple with that predicted from the α, ρ, and κ measurements.

At high temperatures, the accuracy decreases rapidly and it becomes difficult to give a general estimate of the accuracy. As discussed above, the size of the errors and the applicability of the various methods depends on the properties of the material being investigated, the size of the samples available, and the time available for special sample preparation and measurement. In the range of roughly 500 to 800°C, absolute accuracy of better than ±25% are obtained only on materials having rather large thermal conductivity and available in fairly large pieces or at the expense of considerable time and effort on each sample to be measured, and in many cases not even then.

I. DIRECT DETERMINATION OF TZ

Z-Meter

The Z-meter is a simple device which permits the direct determination of the figure of merit TZ or the three parameters α, ρ, and κ. Two current leads and two thermocouples are attached to the sample as shown in Fig. 7.

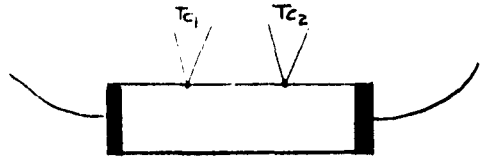

Fig. 7

The sample is suspended by these leads in an evacuated container which is maintained at a constant temperature T_o. When a direct current is passed through the sample, a quantity of heat will be removed from one end of the sample and given up at the other end because of the Peltier effect. A temperature gradient will then be established in the sample and, under steady-state conditions, an equal amount of heat will be conducted from the hot to the cold end. The difference in temperature ΔT is given by the expression

$$\alpha T I_{DC} = \frac{\kappa A \Delta T}{\ell}$$

The difference in voltage between the similar leads of the two thermocouples is the sum of the IR drop and the Seebeck emf.

$$V_{DC} = \alpha\Delta T + I_{DC} \cdot R$$

and the apparent DC resistance that would be measured on the sample is given by the expression

$$R_{DC} = \frac{V_{DC}}{I_{DC}} = \frac{\ell}{A}\left[\frac{\alpha^2 T}{\kappa} + \rho\right]$$

If the resistance is measured with an AC current of 60 cps, there will be no temperature gradient in the material and

$$R_{AC} = \rho \cdot \frac{\ell}{A}$$

Combining these two expressions, we find

$$TZ = \frac{R_{DC} - R_{AC}}{R_{AC}}$$

Thus by simple measuring the resistance with a DC and an AC current, it is possible to determine TZ. If the separate parameters α and κ are desired, it is necessary to determine ΔT in addition to the measurement of R_{AC} and R_{DC}.

In practice, several difficulties are encountered. These are: First, if either of the contacts are poor an extra amount of heat $I^2R_{contact}$ will be generated at one end of the sample and the measurement will be in error. This error can be eliminated in principle by reversing the DC current and averaging the two values of the resistance so obtained. Second, at temperatures where radiation losses become important, the hot end of the sample will lose heat to the container and the cold end will receive heat from the container. A term has been derived to correct for this effect; however, since it involves the emissivity of the sample which is generally not known and the term becomes large as the temperature is raised, the method is limited to modest temperatures. Third, the measurement must be performed in a vacuum and thus is limited to those materials which have low vapor pressures. The same difficulties that were mentioned under diffusivity measurements would arise if an inert gas or a solid insulation were used to prevent the decomposition.

In principle, a thermal guard could be placed around the sample to prevent heat leaks. Such a guard would also permit filling the apparatus with an inert gas to prevent volatilization. However, it would be more difficult to

match the guard in the usual absolute apparatus for the measurement of thermal conductivity.

Small Area Contacts

The method of small area contacts takes advantage of the fact that for a small metal contact embedded in a material and heated or cooled slightly from ambient temperature, the radiation losses are negligible. A typical arrangement is shown in Fig. 8. It consists of the sample mounted on a

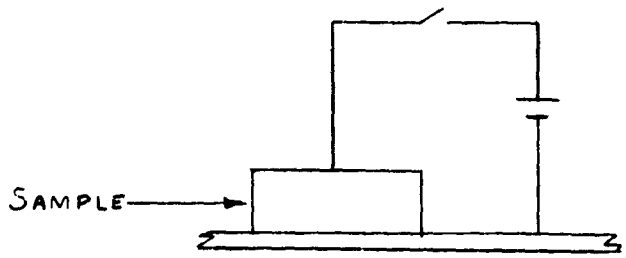

Fig. 8

conducting plate and the small probe which forms the small area contact fused into the sample. In operation, a constant DC voltage V is applied between the probe and the sample. After a steady state equilibrium is established, the voltage is removed and the Seebeck emf δV is measured before it decays significantly. For small TZ, this emf is related to the figure of merit by the equation

$$\delta V = TZ \cdot V + \frac{Z}{2\alpha} \cdot V^2$$

Normally, δV is measured with equal positive and negative applied voltages, and TZ and Z/α calculated by the simple expressions

$$TZ = \frac{\delta V_+ - \delta V_-}{2V} \quad \text{and} \quad \frac{Z}{\alpha} = \frac{\delta V_+ + \delta V_-}{V^2}$$

When $TZ \sim 1$, the Seebeck emf δV will be comparable to V and the equation for δV must be replaced by the expression

$$\delta V = TZ\,(V - \delta V) + \frac{Z}{2\alpha}\,(V-\delta V)^2$$

and this simple quadratic equation must be solved to obtain TZ and Z/α.

The practical problems involved in the determination of TZ by this method are directly involved with the small area contact itself. The only temperature gradients and voltage gradients in the sample are in the vicinity of the contact and the largest gradients are at the contact itself. Under these conditions, the TZ that is determined is that of the material in the vicinity of the contact and primarily that of the material in contact with the metal probe. Thus if the probe should react with the sample, one would measure the properties of the reaction products and not those of the bulk material. If the probe is not fused into the sample but is simply pressed against the surface in order to minimize reaction between the probe and the sample, the method then measures the surface properties of the sample. These may be different from the bulk properties. It is impossible to eliminate these effects other than by the use of a probe material which does not react with the sample, since it is just those large gradients in the vicinity of the contact that make the radiation losses negligible.

Thus a major objection to the small area contact method is that one is not sure a priori what material one is measuring.

am

Scientific Paper 62-121-458-P1 June 19, 1962

THE THERMAL CONDUCTIVITY OF MOLTEN $Cu_2S_{0.25}Te_{0.75}$ AND MOLTEN Cu_2S

by

E. W. Johnson and R. L. Readal

WESTINGHOUSE RESEARCH AND DEVELOPMENT CENTER
Pittsburgh 35, Pennsylvania

THE THERMAL CONDUCTIVITY OF MOLTEN $Cu_2S_{0.25}Te_{0.75}$ AND MOLTEN Cu_2S

by

E. W. Johnson and R. L. Readal

ABSTRACT

A promising liquid thermoelectric material for power conversion applications at temperatures above 1000°C is molten $Cu_2S_{0.25}Te_{0.75}$, developed by J. W. Johnson of Stanford Research Institute. For measuring the thermal conductivity of this material, the apparatus previously used for determining the thermal conductivity of molten Cu_2S was modified and employed. Improved stability of the specimen temperature pattern resulted from the use of a simple, sensitive automatic circuit for stabilizing the 25-100 kw power of the graphite resistance heater. Other modifications improved the versatility and accuracy of the results. Corrections for systematic errors were evaluated in special tests. The thermal conductivity, k, of molten $Cu_2S_{0.25}Te_{0.75}$ at 1040 to 1310°C was found to obey the relation

$$k \text{ (watt/cm deg)} = -0.0326 + 4.50 \times 10^{-5} \, T(°C).$$

The estimated error is $\pm$20%.

Application of the corrections to the data for the thermal conductivity of molten, copper-rich cuprous sulfide at 1100 to 1630°C yielded the relation

$$\log_{10} k \text{ (watt/cm deg)} = 0.306 - 3190/T(°K).$$

These thermal conductivity values are lower than those for molten $Cu_2S_{0.25}Te_{0.75}$ by 0.007 watt/cm deg, while the measured electrical conductivities differ by about 240 $ohm^{-1}cm^{-1}$. The product of absolute temperature and the thermoelectric figure of merit of molten $Cu_2S_{0.25}Te_{0.75}$, as determined by combining the electrical properties subsequently measured at Stanford Research Institute with the thermal conductivity data reported in this paper, is 0.62 at 1100°C.

THE THERMAL CONDUCTIVITY OF MOLTEN $Cu_2S_{0.25}Te_{0.75}$ AND MOLTEN Cu_2S

by

E. W. Johnson and R. L. Readal
Westinghouse Research and Development Center
Pittsburgh 35, Pennsylvania

There is interest in using liquid semiconductors for thermoelectric energy conversion at temperatures above 1000°C. Possible materials for these applications have been studied by Derge, et al (1,2,3,4). Liquid semiconductors related to molten Cu_2S are of particular interest. A promising such material is molten $Cu_2S_{0.25}Te_{0.75}$, developed by J. W. Johnson, et al (5). For this material at 1200°C, Johnson has given the Seebeck coefficient, α, as 170 μv per deg C and the electrical conductivity, σ, as 650 $ohm^{-1}cm^{-1}$. In the present paper we report experimental measurements of the thermal conductivity of this material at 1040 to 1310°C. The paper also presents corrected data for the thermal conductivity of molten copper-rich cuprous sulfide at 1100 to 1630°C.

Experimental

Major elements of the thermal conductivity apparatus. The apparatus and techniques for determining thermal conductivities of liquid semiconductors at temperatures from 1000 to 1800°C have been described (6). We give here a brief summary of the method used in the present experiments. Figure 1 shows the primary elements of the apparatus. The liquid specimen is in contact with both the 5-inch-diameter container and an immersed lid, both of grade AUC graphite. Heat is supplied radiantly from above by a flat graphite resistance heater. The heat is conducted through the specimen and radiated from the container bottom to a graphite radiation shield, which reradiates the heat to a water-cooled metal plate (not shown). The temperatures of the lid, container,

and shield (or receiver) are determined with a micro-optical pyrometer sighted onto the bottoms of small blind holes in the respective members. These temperatures are used to determine both the specimen temperature drop, ΔT, and the thermal flux, F, for use in the relation

$$k = F\,\Delta x/\Delta T \qquad (1)$$

in which k is the thermal conductivity and Δx is the specimen thickness. The flux is computed from the Stefan-Boltzmann equation using the container bottom and shield temperatures and known values of the emissivity of the graphite.

The dashed outline in Fig 1 represents an optional graphite radiation shield between the container bottom and the regular shield. This optional shield was used in a few experiments for reducing the thermal conduction flux.

The left and right sides of Fig 1 are not identical in order that more than a single radial section can be shown. The lid support was electrically insulated from the container support. The former is shown on the left side of Fig 1, and the latter is on the right. Two lids having different diameters of their respective immersed portions were used. The left side of Fig 1 represents the larger-diameter lid, which had an immersed diameter of 4-1/2 inches; this lid had been used in the measurements on Cu_2S (6). The immersed diameter of the smaller lid, represented on the right-hand side of Fig 1, was 3-7/8 inches. The inside diameter of the container was 4-7/8 inches. The specimen thickness was varied by changing the relative heights of the container and lid on their threaded graphite support legs. Both the deep and the shallow pyrometer sighting holes in the lid were aligned beneath the central slot of the graphite resistance heater.

Automatic stabilization of heater power. The thermal conductivity data for molten Cu_2S were scattered due to variations of the heater power with line voltage fluctuations and with slower, thermally caused changes of the heater resistance. To eliminate these difficulties, we used the device in Fig 2 for stabilizing the d.c. power of the graphite resistance heater. The device senses and automatically corrects for deviations of the power from a preset norm. Such deviations may be approximated as differential quantities. Thus, if the heater current is I and the potential drop is E, the requirement that the power remain constant is satisfied if

$$IdE + EdI = 0. \tag{2}$$

A potential V_I proportional to I is obtained from a suitable shunt, and a potential V_E proportional to E is obtained from a voltage divider. The latter is adjustable to permit V_E to be set equal to V_I at each power setting. Eq (2) is then simplified to

$$dV_E + dV_I = 0. \tag{3}$$

The difference signals dV_E and dV_I are obtained from V_E and V_I, respectively, with the aid of bucking potentiometers. The algebraic addition of the difference signals is performed by a "Sigma" Magnetic Amplifier Relay having two input coils and a polarized relay output. The output signals actuate a motor that turns the current-adjustment shaft of one of the Westinghouse RA rectifier welders constituting the main power supply. The sensitivity of response to power fluctuations is $\pm 0.5\%$ and can be improved to $\pm 0.1\%$ by the use of lower-resistance bucking potentiometers.

The precision of the experimental data was significantly improved as a result of stabilization of the heater power. Of each group of temperature readings at a given power level, the maximum deviations from a mean value were usually $\pm 1°C$ or less.

Experimental accuracy of measuring Δx and ΔT. The previous paper (6) reported that the uncertainty of the thermal conductivity measurements on molten Cu_2S was $\pm 25\%$. A major effort was subsequently made to improve the accuracy of the experimental measurements. To determine Δx, gauge blocks were used for adjusting the specimen thickness space between the container and the lid, and after each run the frozen specimen thickness was measured with a micrometer. A shrinkage correction was obtained by comparing the diameters of the frozen specimen and the container. Agreement of the two thickness measurements was within ± 0.01 inch.

For the determination of ΔT, pyrometer readings were taken on the bottoms of the two blind holes of different depths in the lid and extrapolated to yield the temperature of the interface between the specimen and the lid. The same temperature gradient was used for determining the lower interface temperature from the pyrometer reading of the blind hole in the container bottom. A correction is required for the fact that the spectral emissivities of the pyrometer measurement holes are not quite unity, as well as for the possible temperature discontinuities at the interfaces between the molten specimen and the respective graphite members. The former correction was evaluated in an experiment on a solid graphite disc whose thickness was the same as the combined thicknesses of the lid and the container (corresponding to a liquid specimen thickness of zero) and having pyrometer sighting holes

in the top and bottom identical to those in the lid and container. If the hole emissivities had been unity, the values of ΔT obtained from the respective pyrometer readings would have been zero. The ΔT values actually measured were 5° at 1045°C, 7.5° at 1315°C, and 10.5° at 1510°C. These may be used as corrections applicable to the experimentally determined values of ΔT for the pyrometer sighting hole spectral emissivity effect.

The possibility of temperature discontinuities at the specimen-graphite interfaces was examined in experiments on a nearly isothermal "known" specimen of molten copper 0.196 inch thick. The apparent values of ΔT (uncorrected for the emissivity effect) were as high as 22° and as low as 7° in the temperature range between 1100° and 1550°. They exhibited no systematic trend with temperature, but the ΔT values measured after cooling the specimen were often lower, by as much as 14°, than those measured after heating. At the thermal flux values of the experiment, ΔT across the molten copper specimen was computed from electrical conductivity data (7) with the aid of the Wiedemann-Franz law to be 3° at 1100°C and 6° at 1500°. Adding the emissivity correction yields 8.5° at 1100° and 16.5° at 1500° as the expected measured values of ΔT if no interface temperature discontinuity exists. The measured ΔT values were such that the combined interfacial discontinuities could be assigned values up to 12°. An average correction of -10° for ΔT was adopted to compensate for both the emissivity and interface effects. This correction is uncertain to $\pm$8°, which is also the uncertainty of the final ΔT values.

The thickness of the frozen copper specimen was measured after each run to yield the relation between the molten specimen thickness and the spacing of the container and lid at room temperature, using data for the thermal expansivity of copper (8). The resulting estimate of the thickness uncertainty is $\pm$0.006 inch.

Determination of the thermal conduction flux. The thermal conduction flux through the specimen is determined from the steady-state radiant heat flux from the container bottom to the graphite shield immediately below it. The latter flux is computed from the temperatures of the respective graphite members by application of the Stefan-Boltzmann law. The graphite emissivity values employed were those of Jain and Krishnan (9). Plunkett and Kingery (10) have shown that the integrated emissivity of grade AUC graphite increases with surface roughness. Their data bracket those of Jain and Krishnan with good agreement at 1600 to 1800°C in the case of the roughest samples. Both studies showed that the total emissivity of each sample increases with temperature. Since our graphite surfaces were quite rough, their emissivities may have been higher than those of Jain and Krishnan by up to 10%. The estimated uncertainty of the radiant heat flux determination is ±10%.

As a check on the possibility of thermal flux divergence, steady-state temperature measurements were made on the empty specimen container and lid. The thermal flux through the specimen space, F_{tb}, was then wholly radiative. This flux and that between the container bottom and the shield, F_{br}, conform to the relation

$$\frac{F_{tb}}{F_{br}} = \frac{\epsilon_{tb}(T_t^4 - T_b^4)}{\epsilon_{br}(T_b^4 - T_r^4)} \qquad (4)$$

in which T_t is the absolute temperature of the bottom surface of the lid, T_b is the container bottom temperature, T_r is the shield temperature, and ϵ_{tb} and ϵ_{br} are the effective emissivities of the lid-container and container-shield

combinations, respectively. The latter emissivities are defined by, for example,

$$\epsilon_{tb}^{-1} = \epsilon_t^{-1} + \epsilon_b^{-1} - 1 \qquad (5)$$

in which ϵ_t is the emissivity of the graphite at the lower lid surface temperature and ϵ_b is that at the container bottom temperature. Since ϵ increases with temperature it is clear that $\epsilon_{tb}/\epsilon_{br}$ must exceed unity. At the graphite temperatures of our experiments, the values of this ratio computed from the emissivities of Jain and Krishnan were 1.0375 ± 0.0015 when the optional shield was used, and 1.060 ± 0.002 when it was absent.

The quantity $(T_b^4 - T_r^4)/(T_t^4 - T_b^4)$ consists entirely of measured temperatures and is equal to $\epsilon_{tb}F_{br}/\epsilon_{br}F_{tb}$. In the study of molten Cu_2S we assumed that the radiant heat flux between the container bottom and the shield was the same as the conduction flux through the specimen, or that $F_{br} = F_{tb}$. Hence, $\epsilon_{tb}F_{br}/\epsilon_{br}F_{tb}$ would have to exceed unity. We find experimentally, however, that it is between 0.79 and 0.99. Since the emissivity of the graphite probably does not decrease with rising temperature, we must conclude that F_{br} is smaller than F_{tb}. This is probably true whether the specimen space is filled, and the heat transmission is by conduction, or whether it is empty and the heat flow is by radiation. The heat flow paths in the two cases should be most nearly the same when the respective graphite member temperatures are the same, or when the liquid specimen thickness is such that T_t, T_b and T_r are closest to the values observed when the container is empty. A correction for the flux divergence effect may then be obtained from the test data presented in Table I. The sequence of these data is that obtained experimentally, and their form is the same as that of the actual thermal conductivity measurements, where

$$T_m = (T_t + T_b)/2 \tag{6}$$

$$\Delta T = T_t - T_b \tag{7}$$

and

$$R = T_b/T_r. \tag{8}$$

(Due to the temperature gradient in the container bottom, the value of T_b in Eq (8) is slightly smaller than that in Eqs (6) and (7). This difference has been accounted for in the table.) In Table I the measured values of $\epsilon_{tb}F_{br}/\epsilon_{br}F_{tb}$ are given as a function of T_m. We assume that the Jain and Krishnan values of ϵ are correct or that $\epsilon_{tb}/\epsilon_{br}$ is either 1.060 or 1.0375. The resulting values of F_{tb}/F_{br} constitute a correction factor by means of which the conduction flux can be computed from the experimentally determined values of F_{br}.

An additional correction for divergence of the thermal flux through the specimen is required by the fact that the diameter of the lid is smaller than that of the container. This flux divergence could not have occurred in the tests with the empty container and lid. The correction was evaluated by comparing preliminary values of k from runs with both the small- and the large-diameter lids, as will be explained. The result was +5% in the case of the large-diameter lid and +13% in the case of the small lid.

The uncertainties of the correction factors for thermal flux divergence are estimated as $\pm$10% and $\pm$5%, respectively. Since the emissivity uncertainty is $\pm$10%, the error of determining the thermal conduction flux through the specimen is estimated as $\pm$15%.

Results

$Cu_2S_{0.25}Te_{0.75}$. A 4-inch-long, 1100-g cylindrical ingot of $Cu_2S_{0.25}Te_{0.75}$ was received from J. W. Johnson. The initial electrical properties of this material, as measured by Johnson (11), were: α = +172 μv/deg C at 1100°C and 167 at 1200°; σ = 645 $ohm^{-1}cm^{-1}$ at 1100° and 650 at 1200°.

The ingot was remelted and cast under argon in a graphite crucible having the same bottom contour as the specimen container (Fig. 1) and situated in the space normally occupied by the specimen assembly beneath the graphite resistance heater of the thermal-conductivity apparatus. The resulting casting was in the form of a disc, which was broken through the center to form two nearly equal-size specimens, A and B. These were remelted and cast in the crucible to form specimen-shaped discs. After four measurement runs on Specimen A and three on B, a "thick" specimen was made by combining A with 40% of B in the crucible, and the remainder of B became a "thin" specimen. The results of all runs are listed in Table II, where k' represents the preliminary or uncorrected thermal conductivity values determined in the same way as the previous results for molten Cu_2S (6).

The k' values were corrected in three stages to yield values of the thermal conductivity k. First, a correction of 10° was subtracted from each ΔT value listed in the table and k' was recomputed. Next, the factor F_{tb}/F_{br} was obtained from a plot of the values listed in Table I, and this was multiplied by k'. The results were plotted against $(\text{lid diameter/container diameter})^2$ and extrapolated to unity to determine the correction factor for divergence of the thermal conduction flux within the specimen. This factor, which was found to be 1.05 in the case of the large lid and 1.13 in the case of the small lid, was multiplied by the corrected k' values to yield the final values of k. These are listed in Table II.

Each measurement run consisted of three to five steps, in each of which a thermal steady state was maintained while the temperatures of the lid, container, and shield were measured in turn several times. In some runs the measured value of k was found to be consistently higher after cooling the specimen than after heating it. This thermal hysteresis effect was strongest at the lowest temperatures in the absence of the optional shield, being manifested as a lack of reproducibility of ΔT. The same effect was seen in the tests on molten copper. The values of k measured after heating were graphically averaged with those after cooling to yield the values of k considered to be the most probable. The largest deviation from this average was $\pm 10\%$.

A plot of the results of all twelve measurement runs is presented in Fig 3. For the preparation of this graph, a plot of k against T_m was first made for each run. All but two such plots could be satisfactorily represented by straight lines. A pair of locations on and near the ends of each line was then selected and replotted as the points in Fig 3. (If the original plot was not linear, three representative points were taken.) The points in Fig 3 thus represent the extremities of the plotted lines resulting from the various runs.

It is clear that the measured values of k from four of the runs are significantly lower than those from the other eight. The latter consisted of all runs with the thin and medium-thickness specimens and with the regular receiver shield. The straight line in Fig 3 represents only these data, its equation being

$$k \text{ (watt/cm deg)} = -0.0326 + 4.50 \times 10^{-5} \, T(^\circ C). \qquad (9)$$

Of the four runs yielding k values below the line, two were with the thick specimen and the other two were with the optional shield. In all four

cases ΔT was larger than it had been in the corresponding tests on the empty container and lid, and therefore the values of the flux divergence correction employed may have been incorrect. On the other hand, the values of ΔT and R obtained in the tests with the empty container and lid and with the regular shield are bracketed by the data on the thin and medium-thickness specimens. This is the main reason for our drawing the line in Fig 3 to represent only the latter data.

Following the thermal-conductivity measurement runs, the thin specimen was returned to J. W. Johnson for remeasurement of its electrical properties. The results (13) indicate that both the electrical resistivity and the Seebeck coefficient changed significantly while the sample was in our possession. The final resistivity as a function of temperature is represented by Johnson as a straight line between 4.45 milliohm cm at 1000°C and 3.1 at 1200°. The corresponding resistivity increase (relative to the initial measurements) is a factor of 2.8 at 1000° and 2.0 at 1200°. The final values of the Seebeck coefficient are represented as varying linearly with temperature from 195 μv/deg at 1000° to 146 at 1200°.

These changes of the electrical properties may be due to chemical changes of the sample in the thermal conductivity apparatus, although this possibility has not, to our knowledge, been confirmed by chemical analyses. Of more practical concern is the question of whether the thermal conductivity data in Table II are representative of the sample in its "initial" or its "final" condition. From the fact that there is no discernible trend of the data with the sequence of the measurements, as well as from other evidence to be discussed, we must conclude that the material was in its "final" condition at all times during these measurements.

Corrected data for the thermal conductivity of molten Cu_2S. The values of the thermal conductivity of molten copper-rich cuprous sulfide presented previously (6) were obtained in the same way as the present data for k'. The large-diameter lid was used with the regular shield in measurements on both a thin and a thick specimen. The respective corrections are now applied to these k' data, and the results are presented in Table III. These values of k were plotted against T_m. In the temperature range common to both liquids, viz., 1100 to 1300°C, the best curve through the points was below and essentially parallel to that for $Cu_2S_{0.25}Te_{0.75}$, the difference being 0.0070 watt/cm deg. Below 1300°C, then, the thermal conductivity of molten Cu_2S is represented by

$$k \text{ (watt/cm deg)} = -0.0396 + 4.50 \times 10^{-5} \, T(°C). \qquad (10)$$

We found previously (6) that the data over the temperature range 1100 to 1630°C were best represented by an exponential relation of the form of Eq (11). The corrected data were replotted as log k against 1/T, and the straight line best representing them had the equation

$$\log k \text{ (watt/cm deg)} = 0.306 - 3190/T(°K). \qquad (11)$$

Discussion

Acceptance of the present thermal conductivity values depends upon the accuracy of the experimental measurements of Δx, ΔT, and F. The thickness Δx is easily measured and is known to remain constant within small limits. The range of observed values of ΔT was 153 to 409° in the case of the molten specimen materials, while the tests with molten copper yielded ΔT values as low as 7°. The latter values were used in the formulation of a subtractive correction to yield final values of ΔT of accuracy comparable to that of Δx.

In the determination of the thermal conduction flux, F, the employed values of the total emissivity of the graphite may be in error by as much as 10%. Another uncertainty originates from the divergence of the heat flux both within the specimen and in the radiation space between the container bottom and the shield. The correction for the latter divergence is as high as 31%. All of these corrections are in such a direction as to cause k to exceed k'. The uncertainty of the final k values is estimated as $\pm$20%.

The thermal and electrical conductivities are related to each other through the Lorenz number, L, defined by

$$k = \sigma LT. \tag{12}$$

The value of L found in metals is approximately 2.5×10^{-8} volt^{2}deg^{-2}. Considerably larger values of L may occur in semiconductors having ambipolar conduction, and it appears that molten copper-rich cuprous sulfide is such a material. Its electrical conductivity rises with temperature at a rate consistent with a carrier activation energy of 0.7 ev (1). Two independent measurements of the electrical conductivity of this material (1,12) have yielded an average σ value of 64 ohm^{-1}cm^{-1} at 1200°C. Since our measured value of the thermal conductivity at this temperature is 0.014 watt/cm deg, the apparent Lorenz number is 14.5×10^{-8} volt^{2}deg^{-2}. Both the high value of L and the fact that σ rises exponentially with temperature are evidence of ambipolar conduction in molten Cu_2S.

Quite a different situation characterizes molten $Cu_2S_{0.25}Te_{0.75}$, at least in its "initial" condition. There, the fact that the temperature coefficient of the electrical conductivity is essentially zero (5, 11) is evidence that ambipolar conduction is lacking.

The present thermal conductivity data probably apply to the material in only its "final" condition (13), where the Seebeck coefficient decreases and both the electrical and thermal conductivities increase with increasing temperature. This behavior is qualitatively similar to that of molten Cu_2S. The apparent activation energy derived from the slopes of plots of both log σ and log k against $1/T$ is 0.36 ± 0.04 ev. The calculated Lorenz number is 4.64×10^{-8} $volt^2deg^{-2}$ at 1100°C and 4.46×10^{-8} at 1200°. The fact that these values of L seem reasonable, as well as the good agreement of the temperature dependencies of the final values of σ and k, constitutes additional evidence that the material was in only its "final" condition during all the thermal conductivity measurements.

The product of the thermoelectric figure of merit, Z, and absolute temperature, T, is equivalent to α^2/L. The thermal conductivity data in Fig 3 have been used by J. W. Johnson (13) for computing values of ZT of molten $Cu_2S_{0.25}Te_{0.75}$ in three conditions: the "initial" and "final" states of the sample examined by us and the "initial" state of a subsequently prepared sample. (The latter sample had essentially the same electrical resistivity as had the previous sample in its initial state, but the Seebeck coefficient was lower by about 12 μv/deg.) Our view is that two of Johnson's three computations of ZT are incorrect, because the (as yet unknown) factors responsible for decreasing σ during the time between the initial and final electrical property measurements must have had a similar effect on k. The highest ZT value proposed by Johnson (13) is 1.98 at 1000°C. The corresponding Lorenz number has the surprisingly low value of 1.53×10^{-8} $volt^2deg^{-2}$.

From the available data we conclude that a valid estimate of ZT can now be made for only the material in its "final" condition in the temperature range 1070 to 1200°C. The results are 0.69 at 1070°, 0.62 at 1100°, and 0.48 at 1200°.

These figures are in substantial agreement with those given by Johnson (13) for the same conditions.

The changes of properties that apparently occurred while the material was being prepared by us for measurement in the thermal conductivity apparatus are dismaying and should be further investigated. Reliable data for the thermal conductivity and figure of merit of the material in its "initial" condition would be especially valuable, since these quantities are almost certainly more favorable than the existing data for the "final" state. The measurements may only be possible, however, after the response of the material to its environment at high temperatures has been better studied and controlled. Since the design of the thermal conductivity apparatus resembles in certain ways that of envisioned thermoelectric generators employing liquids at temperatures above 1000°C, any improvement of this apparatus would probably benefit also the final generator design.

Acknowledgments

The work reported in this paper was supported by the U. S. Department of the Navy, Bureau of Ships, Contract NObs-84317. Dr. Roland Ure kindly reviewed the manuscript and made helpful suggestions.

References

1. M. Bourgon, G. Derge, and G. M. Pound. Conductivity and Sulfur Activity in Liquid Copper Sulfide. Trans. AIME (1957), p. 1454, Journal of Metals (November 1957).

2. D. F. Stoneburner, Ling Yang, and G. Derge. Measurement of the Thermoelectric Power of Several Molten Sulfide-Solid Tungsten Thermocouples. Trans. AIME (1959), vol. 215, p. 879.

3. D. Argyriades, G. Derge, and G. M. Pound. Electrical Conductivity of Molten FeS. Trans. AIME (1959), vol. 215, p. 909.

4. D. F. Stoneburner. Thermoelectric Power and Electrical Conductivity of Molten Binary Thallium Alloys. Paper No. 7 of Session IV of Joint Technical Society and Department of Defense Symposium on Thermoelectric Energy Conversion, Dallas, Jan. 9-12, 1961.

5. J. W. Johnson. Thermoelectric Materials. Bimonthly Progress Report No. 13 from Stanford Research Institute to U. S. Department of the Navy, Bureau of Ships. Contract No. NObs-77017 (Feb. 28, 1961).

6. E. W. Johnson and R. L. Readal. Measurement of Thermal Conductivities of Liquid Thermoelectric Materials (Molten Cuprous Sulfide) from 1000° to 1800°C. Advanced Energy Conversion, vol. 1 (1962).

7. E. F. Northrup. Resistivity of Copper in Temperature Range 20°C to 1450°C. J. Franklin Inst., vol. 177, 1 (1914).

8. A. Goldsmith, T. E. Waterman, and H. J. Hirschhorn. Handbook of Thermophysical Properties of Solid Materials. Volume 1. The MacMillan Company, New York, 1961.

9. S. C. Jain and K. S. Krishnan. The Distribution of Temperature along a Thin Rod Electrically Heated in vacuo. Proc. Roy. Soc. (1954), vol. A225, p. 7.

10. J. D. Plunkett and W. D. Kingery. The Spectral and Integrated Emissivity of Carbon and Graphite. Proceedings of the Fourth Carbon Conference (at University of Buffalo), New York, Pergamon Press (1960), p. 457.

11. J. W. Johnson. Private communication.

12. J. W. Johnson. Thermoelectric Materials. Bimonthly Progress Report No. 7 from Stanford Research Institute to U. S. Department of the Navy, Bureau of Ships. Contract No. NObs-77017 (Feb. 17, 1960).

13. J. W. Johnson. Thermoelectric Materials. Bimonthly Progress Report No. 20 from Stanford Research Institute to U. S. Department of the Navy, Bureau of Ships. Contract No. NObs-77017 (July 17, 1962).

THE THERMAL CONDUCTIVITY OF MOLTEN $Cu_2S_{0.25}Te_{0.75}$ AND MOLTEN Cu_2S

E. W. Johnson and R. L. Readal

Figure Captions

Fig 1 Specimen Assembly

Fig 2 Diagram of automatic d-c power regulation system

Fig 3 Thermal conductivity of molten $Cu_2S_{0.25}Te_{0.75}$

DWG 624A459

Table I.—Results of Test Runs on Empty Specimen Container and Lid

Run No., Lid, Shield	T_m (°C)	ΔT (°C)	R	$\frac{\varepsilon_{tb} F_{br}}{\varepsilon_{br} F_{tb}}$	$\frac{F_{tb}}{F_{br}}$
Run I	1288	188	1.203	0.886	1.195
Lge., Reg	1146	179	1.206	0.837	1.269
	1410	197	1.202	0.925	1.146
	1510	205	1.197	0.939	1.128
	1159	177	1.205	0.857	1.239
Run II	1330	135	1.107	0.893	1.163
Lge., Opt.	1154	126	1.107	0.828	1.252
	1456	137	1.109	0.991	1.046
Run III	1059	121	1.106	0.795	1.307
Lge., Opt.	1142	126	1.107	0.826	1.257
	1360	137	1.109	0.911	1.139
	1318	130	1.108	0.935	1.108
	1230	131	1.105	0.839	1.237

DWG 29581B2

Table II.—Results of Thermal Conductivity Measurements on Molten $Cu_2 S_{0.25} Te_{0.75}$

Run No., Specimen, Thickness, Lid, Shield	T_m (°C)	ΔT (°C)	R	$10^3 k'$ (w/cm deg.)	$10^3 k$ (w/cm deg.)
Run 1, A	1170	244	1.183	14.6	19.9
0.73 cm,	1250	260	1.181	17.1	22.7
Lge. Reg.	1307	255	1.178	20.7	26.9
	1142	226	1.179	14.7	20.3
Run 2, A	1078	247	1.173	10.3	14.6
0.73 cm.	1147	240	1.182	13.9	19.1
Lge., Reg.	1224	248	1.180	16.7	22.4
	1093	229	1.184	12.5	17.6
Run 3, A	1081	266	1.173	9.4	14.2
0.73 cm.	1234	267	1.176	15.3	21.9
Sm., Reg.	1171	250	1.179	13.9	20.3
	1085	237	1.181	11.5	17.5
Run 4, B	1144	211	1.194	12.3	18.3
0.53 cm.	1217	213	1.191	15.1	21.9
Sm., Reg.	1084	195	1.198	11.3	17.4
Run 5, A	1118	190	1.095	10.4	14.6
0.70 cm	1048	181	1.099	9.1	13.2
Lge., Opt.	1182	202	1.094	11.8	16.1
	1280	211	1.096	15.2	19.6
	1127	192	1.094	10.5	14.7
Run 6, B	1122	181	1.099	11.6	16.3
0.69 cm.	1049	176	1.101	9.5	13.9
Lge., Opt.	1252	200	1.096	14.9	19.6
	1197	193	1.096	13.1	17.7
	1126	182	1.097	11.4	16.1
Run 7, B	1063	243	1.172	9.3	13.2
0.69 cm.	1163	233	1.181	14.2	19.4
Lge., Reg.	1248	244	1.181	17.4	23.1
	1088	224	1.184	11.9	16.8
Run 8, Thick	1184	325	1.163	12.9	18.6
1.01 cm.	1106	305	1.158	10.7	15.9
Sm., Reg.	1253	348	1.161	14.3	20.1
	1189	324	1.163	13.1	18.9
Run 9, Thick	1189	336	1.162	12.4	17.8
1.01 cm.	1107	324	1.163	10.0	14.9
Sm., Reg.	1224	337	1.164	13.8	19.7
	1188	329	1.161	12.7	18.3
Run 10, Thin	1158	158	1.208	14.4	20.2
0.39 cm.	1074	153	1.211	11.6	16.9
Lge., Reg.	1269	167	1.206	18.7	25.1
	1233	164	1.205	17.1	23.3
	1125	153	1.209	13.6	19.3
Run 11, Thin	1156	169	1.208	13.1	19.7
0.39 cm.	1058	166	1.214	10.1	15.8
Sm., Reg.	1267	174	1.204	17.5	25.3
	1224	173	1.206	15.7	23.0
	1122	164	1.209	12.4	18.9
Run 12, Thin	1065	164	1.208	10.4	15.1
0.40 cm.	1131	166	1.205	12.6	17.7
Lge., Reg.	1211	172	1.202	15.2	20.8
	1116	162	1.205	12.4	17.6
	1068	162	1.209	10.7	15.5

DWG 624A460

Table III.–Corrected Results of Thermal Conductivity Measurements on Molten Cu_2S

Run No., Specimen, Thickness	T_m (°C)	ΔT (°C)	R	$10^3 k'$ (w/cm deg.)	$10^3 k$ (w/cm deg.)
Run 16	1039	317	1.204	5.0	7.1
Thin, 0.48 cm.	1253	222	1.202	14.9	19.8
Run 19	1086	264	1.190	6.7	9.4
Thin,	1285	270	1.194	12.3	16.0
0.48 cm.	1384	292	1.190	14.4	18.1
	1525	275	1.207	24.1	29.5
	1629	258	1.202	32.5	39.6
Run 20	1471	367	1.190	26.7	32.7
Thick,	1358	355	1.178	19.9	25.0
0.95 cm.	1225	334	1.162	13.2	17.5
	1100	365	1.151	7.3	10.1
Run 23	1505	240	1.203	27.8	34.3
Thin,	1401	245	1.197	19.9	25.0
0.48 cm.	1261	245	1.188	12.8	16.9
Run 24	1325	315	1.181	21.1	27.0
Thick,	1425	380	1.163	19.8	24.4
0.95 cm.	1507	409	1.154	21.2	25.7
	1399	361	1.155	19.3	24.0

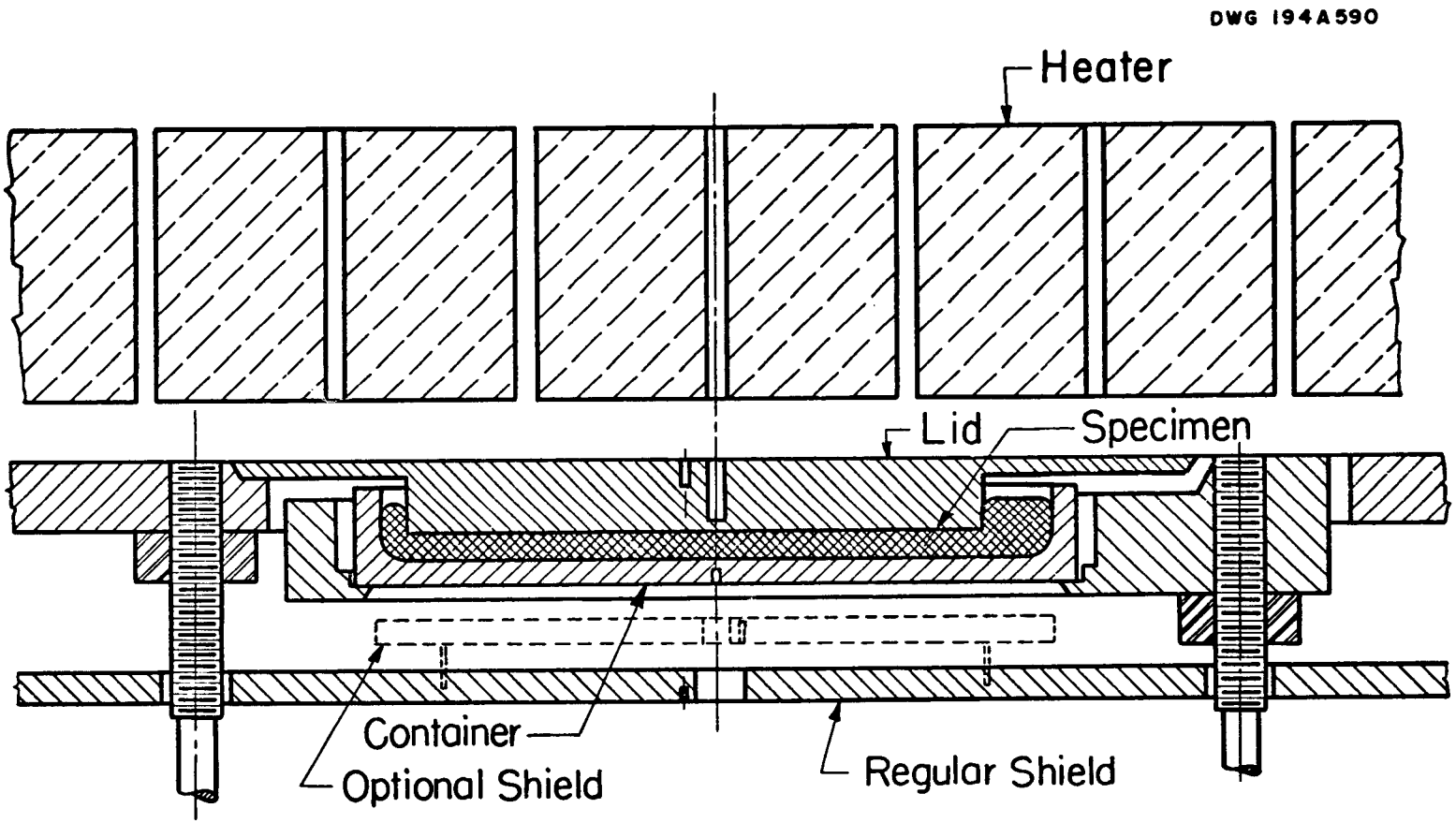

Specimen Assembly.

Fig. 1

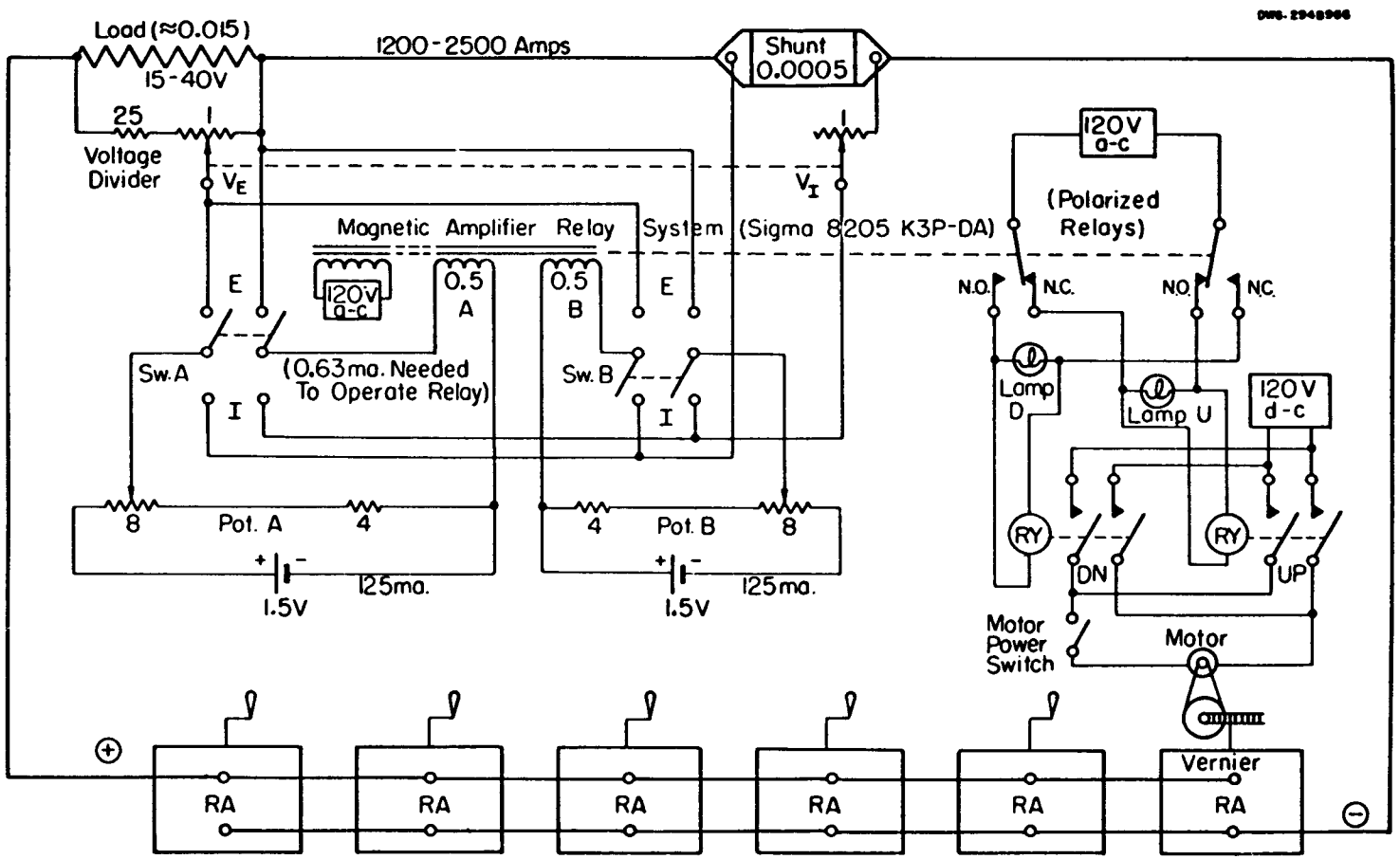

Fig. 2 Diagram of automatic d-c power regulation system.

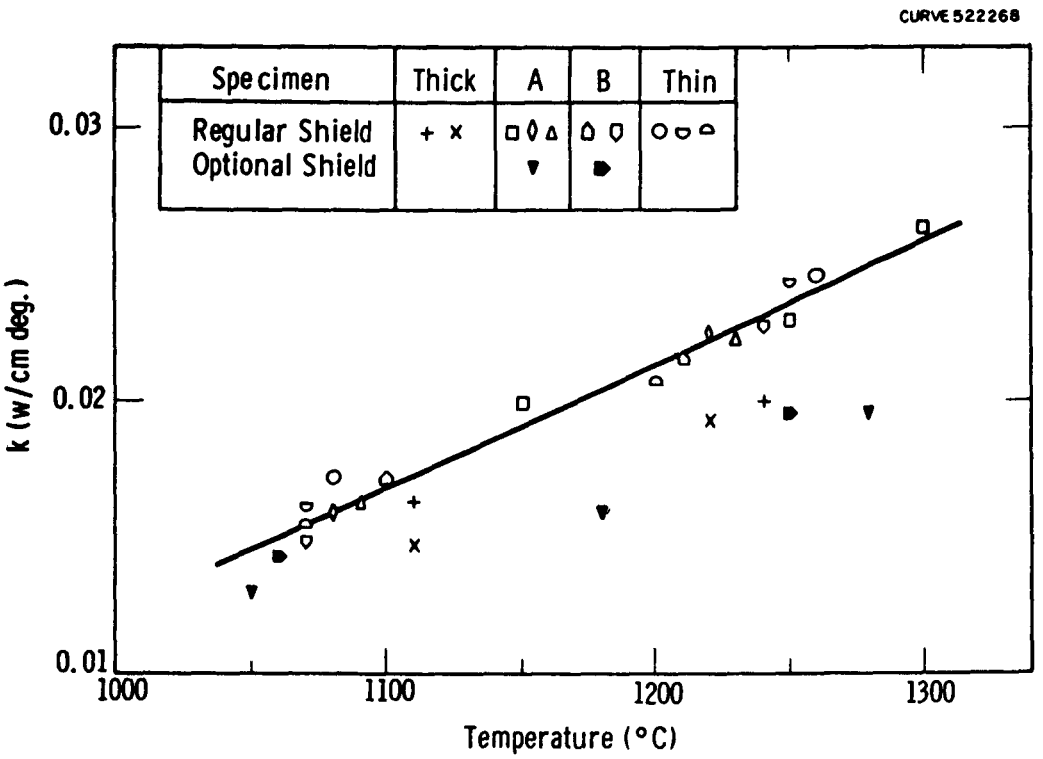

Fig. 3.—Thermal conductivity of molten $Cu_2 S_{0.25} Te_{0.75}$